

Robust Catalysis on 2D Materials Encapsulating Metals: Concept, Application, and Perspective

Jiao Deng, Dehui Deng,* and Xinhe Bao*

Great endeavors are undertaken to search for low-cost, rich-reserve, and highly efficient alternatives to replace precious-metal catalysts, in order to cut costs and improve the efficiency of catalysts in industry. However, one major problem in metal catalysts, especially nonprecious-metal catalysts, is their poor stability in real catalytic processes. Recently, a novel and promising strategy to construct 2D materials encapsulating nonprecious-metal catalysts has exhibited inimitable advantages toward catalysis, especially under harsh conditions (e.g., strong acidity or alkalinity, high temperature, and high overpotential). The concept, which originates from unique electron penetration through the 2D crystal layer from the encapsulated metals to promote a catalytic reaction on the outermost surface of the 2D crystal, has been widely applied in a variety of reactions under harsh conditions. It has been vividly described as “chainmail for catalyst.” Herein, recent progress concerning this chainmail catalyst is reviewed, particularly focusing on the structural design and control with the associated electronic properties of such heterostructure catalysts, and also on their extensive applications in fuel cells, water splitting, CO₂ conversion, solar cells, metal–air batteries, and heterogeneous catalysis. In addition, the current challenges that are faced in fundamental research and industrial application, and future opportunities for these fantastic catalytic materials are discussed.

1. Introduction

In the fields of catalytic science and technology, developing catalysts with high activity and stability is eternally the major pursuit. In consideration of this motivation, precious metals (e.g., Pt, Pd, Au, and their alloys) are always employed to drive most of catalytic processes because they can exhibit inimitable

performance beyond many other catalytic materials in the heterogeneous catalysis,^[1–3] electrocatalysis,^[4–6] and photocatalysis.^[7–9] However, precious-metal catalysts all suffer from the disadvantages of high cost and limited reserve on the earth, determining that they are not viable for large-scale industrial applications. Hence, seeking for alternatives with nonprecious-metal catalysts has become a hot topic in the catalytic field. Although nonprecious-metal catalysts owned the comparable or surpassing catalytic capacity in some featured reaction systems,^[10–12] the survival environment of numerous catalytic reaction is badly difficult for the nonprecious-metal catalysts, and even sometimes for precious metals. For example, many harsh conditions such as the strong acidic or alkaline medium in liquid reaction, high overpotential in electrocatalysis, and high temperature in gas-solid catalytic system easily lead to corrosion, oxidation, or sintering of the metal catalysts. Therefore, keeping high stability of metal catalysts especially the nonprecious-metal catalysts without sacrificing

their activity under harsh conditions is an urgent task, but it remains a great challenge.

Recently, a novel and promising strategy has been proposed by our group to overcome the low stability of nonprecious-metal catalysts operated under harsh reaction conditions,^[13–16] i.e., designing and fabricating the unique chainmail catalyst via graphene shell completely encapsulating transition metals (TMs). In the chainmail catalyst, the electron of TMs can penetrate through the graphene shell to promote the catalytic reaction on the external graphene surface, while the graphene shell can completely prevent reaction molecules and medium from contacting the TMs and therefore can protect the TMs from damage in harsh conditions. It will improve both the activity and stability of nonprecious-metal catalysts.^[13] Since then, vast structural designs and modulations in such chainmail catalysts have been developed, involving of encapsulating different materials of metallic TMs, TM alloys, TM carbides, TM oxides, TM phosphides, and TM nitrides, as well as employing different shells of graphene, boron nitride, graphitic carbon nitride, and TM dichalcogenides for the encapsulation. This chainmail catalyst delivers a novel concept and offers a future opportunity for the nonprecious-metal catalysts to be utilized in many catalytic reactions under harsh conditions, and also offers a good model

Dr. J. Deng, Prof. D. Deng, Prof. X. Bao
State Key Laboratory of Catalysis
Collaborative Innovation Center of Chemistry for Energy Materials (iChEM)
Dalian Institute of Chemical Physics
Chinese Academy of Science
Dalian 116023, China
E-mail: dhdeng@dicp.ac.cn; xhbao@dicp.ac.cn

Dr. J. Deng, Prof. D. Deng
State Key Laboratory of Physical Chemistry of Solid Surfaces
Collaborative Innovation Center of Chemistry
for Energy Materials (iChEM)
College of Chemistry and Chemical Engineering
Xiamen University
Xiamen 361005, China

DOI: 10.1002/adma.201606967

for flexible tuning of structural and electronic properties in such kind of catalysts.

Here, we briefly summarize recent progress in the TM-2D crystal chainmail catalysts and their wide applications in a number of chemical reactions. We introduce the concept of electron penetration originated from the TM-graphene structure, and then various pathways to tune its structure, components, and electronic state, so as to optimize the catalytic performance of this unique catalyst. On this basis, the different applications of the chainmail catalysts via structural control are systematically discussed (Table 1). Finally, we give a perspective on challenges and opportunities in future research with respect to both the fundamental understanding and industrial application of such chainmail catalysts.

2. The Concept of Chainmail for Catalyst

2.1. Origin from the TM@Graphene Catalyst

Nonprecious-metal catalysts with TMs in their low valence state can even display higher reactivity in many reactions than some precious metals, but they usually do not demonstrate sustainable reactivity for many reactions under harsh conditions, such as strong acidic or alkaline medium, high overpotential, and high temperature.^[15] In many enzymes and homogeneous catalysts, coordinatively unsaturated (CUS) metal sites are often the catalytically active sites and also are very stable due to the effective protection by the different ligands.^[17,18] For example, in the methane monooxygenase (MMO), the converted reaction of methane to methanol typically occurs on a di-iron center, in which the TMs are constrained by the proteins to prevent their deep oxidation during catalysis and thereby the CUS sites are effectively maintained.^[17] Inspiring from the nature, other substance with the similar function to the organic ligands in enzymes may be explored to protect the unstable TMs.

Graphene, one of 2D materials, with unique physical and chemical properties is very stable under harsh conditions,^[19–25] which is an excellent candidate for the protection. For example, previous studies have reported that graphene can stabilize some metal-based structures like the metal atoms doped into a graphene matrix^[26–28] or the well-known metal/nitrogen/carbon composites.^[29–34] However, the stability is still not satisfied under harsh conditions, due to the weak bonding between metals and carbon atoms or the direct exposure of metals to the harsh environment. One promising strategy is to employ graphene as outer shell to completely encapsulate metals, which can effectively protect the inside metals from being destroyed in harsh conditions because the inside metals cannot contact reactants and the reaction medium.

The remaining key point is how to trigger the catalytic activity of these materials. Pristine graphene is a zero-overlap semimetal with very low density of states (DOS) near the Fermi level, which is actually very inert in reaction.^[19,35] Therefore, in order to increase the reactivity of graphene, it needs to increase the DOS near the Fermi level.^[36] Like the chemical modification with dopants such as nitrogen and boron to increase the DOS near Fermi level of graphene,^[37,38] the CUS metals inside the graphene shells with sufficient electrons can be used as



Jiao Deng received his B.S. degree in chemistry from Sichuan University in 2010 and his Ph.D. in physical chemistry from Dalian Institute of Chemical Physics (DICP), Chinese Academy of Sciences (CAS) in 2015. Following that, he served as an iChEM postdoctoral fellow at Xiamen University. His research is focused on the

design and development of novel nonprecious-metal catalysts for energy-related catalysis, including the fundamental research of graphene, MoS₂, etc. 2D materials.



Dehui Deng received his B.S. in Light Industry Engineering and B.S. in National Economy Management from Sichuan University in 2007 and Ph.D. in physical chemistry from DICP, CAS in 2013. He subsequently joined State Key Laboratory of Catalysis, DICP as an Associate Professor, and became a Full Professor

in 2017. Since January 2015, he has served as an iChEM Professor at Xiamen University. He also served as a visiting scholar at Stanford University between 2015 and 2016. His research interests include the development of nonprecious-metal catalysts and fundamental research in heterogeneous catalysis and electrocatalysis.



Xinhe Bao received his Ph.D. in physical chemistry from Fudan University in 1987. He held an Alexander von Humboldt Research Fellow position at the Fritz-Haber Institute, Berlin, between 1989 and 1995. Following that, he joined DICP as a full Professor. He became a member of the CAS in 2009. His research interests

are in nano- and interfacial catalysis, focusing on the fundamental understanding of heterogeneous catalysis, including the development of new catalysts and novel catalytic processes related to energy conversion and storage.

electron donors for tuning the electronic state of graphene surface. Encouragingly, previous studies showed that the electron transfer will happen when fullerenes or metallofullerenes were embedded into the carbon nanotube, and thereby it will change the local surface electronic state of the carbon nanotube.^[39,40]

Table 1. Summary of chainmail catalysts for application in catalysis.

Chainmail catalyst	Structure	Reaction system	Performance
TM@graphene	FeCo alloy encapsulated in N-doped CNT	ORR in PEMFCs ^[45]	Maximum power density of 328 mW cm ⁻² , and stability of more than 150 h
	CoNi alloy encapsulated in ultrathin graphene shell (1–3 layers)	HER in acidic medium ^[46]	Overpotential of 142 mV at 10 mA cm ⁻²
	FeNi encapsulated in single-layer graphene shell	OER in alkaline medium ^[49]	Overpotential of 280 mV at 10 mA cm ⁻²
	Fe encapsulated by ultrathin (1–3 layers) carbon layers	CO ₂ conversion ^[156]	CO generation of 55.75 μmol min ⁻¹ , selectivity of 99.76%
	FeNi encapsulated in N-doped pod-like CNT	CE of DSSCs ^[160]	Power conversion efficiency of 8.82%
	Carbon-encapsulating NiFe ₂ nanocrystals	Zn–air battery ^[169]	Charge–discharge overpotential of 0.78 V at 50 mA cm ⁻²
	N-doped single layer graphene shell encapsulating Co	Li–air battery ^[177]	Discharge and charge overpotentials of 0.14 and 0.58 V
TM carbide@graphene	Fe nanoparticles encapsulated in pod-like carbon nanotubes	Fischer–Tropsch synthesis ^[188]	High selectivity of light olefins (45%) and high stability over 120 h reaction
	Hierarchically porous N-doped carbon frameworks embedded with Co nanoparticles	Catalytic hydrogenation ^[181]	Rate constant of 1.024 min ⁻¹ for the hydrogenation of 4-aminophenol
TM carbide@graphene	Ultrasmall Mo ₂ C nanoparticles embedded within nitrogen-rich carbon (NC) nanolayers	HER over a wide PH range ^[145]	Overpotential of 124, 156, and 60 mV at 10 mA cm ⁻² in acidic, neutral, and basic medium, respectively
TM oxide@graphene	Uniform CoMnO nanoparticles coated with a thin, continuous nitrogen-doped carbon (CN) framework	HER in alkaline medium ^[60]	Overpotential of 71 mV at 20 mA cm ⁻²
TM phosphide@graphene	Co ₂ P encapsulated in N,P-doped graphene	HER in acidic medium ^[65]	Overpotential of 103 mV at 10 mA cm ⁻²
TM nitride@graphene	Hybrid Co ₂ P and CoxN nanoparticles encapsulated in N-doped graphene shell	Zn–air battery ^[67]	Charge–discharge voltage gap of 0.85 V
TM@g-CN	Carbon nitride (CN) encapsulating Ni	Catalytic hydrogenation ^[78]	Conversion and selectivity of 100% in hydrogenation of <i>p</i> -nitrobenzoic acid under pH of 3.6 for 4 h
	Metallic Co encapsulated in nitrogen-rich carbon nitride	HER in acidic medium ^[79]	Overpotential of 200 mV at 10 mA cm ⁻²
TM oxide@g-CN	C ₂ N 2D network encapsulating Co oxide	NaBH ₄ hydrolysis in alkaline medium ^[80]	Maximum H ₂ generation rate of 8903 mL min ⁻¹ g ⁻¹ at 303 K
TM@BN	BN covered Au	ORR in acidic medium ^[74]	Overpotential reducing by ≈ 0.27 V if BNNS is placed on Au
TM@MoS ₂	Single-layer MoS ₂ attached on different substrates of Ir (111), Pd (111), and Ru (0001)	Hydrogen adsorption ^[75]	Binding of hydrogen enhanced as much as ≈0.4 eV by DFT calculation

For example, the bandgap of carbon nanotube is narrowed to ≈0.1 from ≈0.5 eV where Gd@C₈₂ endohedral fullerenes are inserted.^[39] Moreover, several theoretical calculations have exhibited that when TMs like Fe, Co, and Ni were encapsulated in graphene shells, electron transfer will happen through the metal–carbon interaction.^[41,42] For example, inserting TM nanowires inside zigzag nanotubes *C*(*m*, 0) will bring charge transfer from TMs to carbon nanotubes, and the transfer process will be enhanced via decreasing the nanotube diameter and increasing nanowire thickness.^[41] However, whether the electron transfer from CUS TMs can affect the catalytic reactions on graphene surface has not been investigated and understood before, though some similar structures of graphitic carbon coating metal can be found in several catalytic systems.^[43,44]

In light of this, the definite concept about the electronic effect between nonprecious-metal catalyst and graphene shell on the catalysis has been proposed by our group recently (Figure 1a).^[13] We constructed a well-defined structure by completely encapsulating CUS metal into graphene shell, and found

that oxygen reduction activity in the acidic medium on graphene surface has been significantly enhanced assisting by the encapsulated metallic Fe nanoparticles (Figure 1b). The stability of the Fe catalyst, usually suffered from acidic solutions, oxidants or poisons, has been significantly improved. Meanwhile, the high activity can be effectively maintained. Experiments and theoretical calculations showed that because of the work function difference between the graphene and Fe, a part of electron will transfer from the Fe to the graphene surface. It leads to the decrease of local work function on graphene surface (Figure 1c), which further increases the DOS near Fermi level of graphene (Figure 1d,e) and therefore promotes the oxygen activation on graphene surface to enhance the catalytic activity. This strategy is like soldiers wearing chainmail to protect themselves from injury in ancient combat, where the chainmail should not hinder the fighting capacity of soldiers. So the concept can be vividly depicted as “chainmail for catalyst” (Figure 1f), in which the graphene shells are used to stabilize nonprecious-metal catalysts under harsh conditions and the electronic properties for

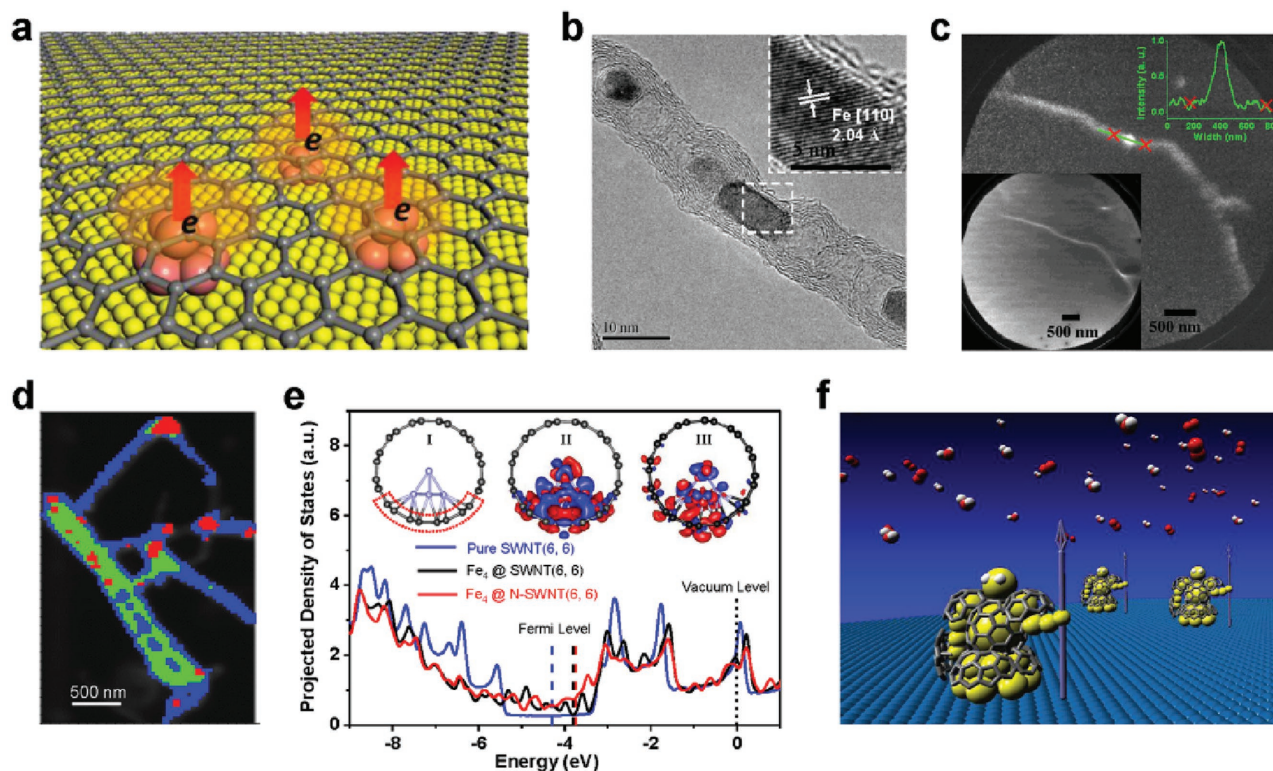


Figure 1. a) Schematic illustration of electron penetration through graphene layer for catalysis. b) HRTEM image of Pod-Fe with the inset showing Fe [110] crystal face of the nanoparticles. c) Photoemission electron microscopy (PEEM) image of Pod-Fe with a start voltage of 1.7 V for its laser. The top inset showing the lightness profile along the lines. The bottom inset showing the corresponding low-energy electron microscopy (LEEM) image of the same region. d) STXM chemical images of the Pod-Fe, red: iron particle regions, green: thick CNT regions, blue: thin CNT regions. e) Projected density of p-states of carbon atoms bonded to Fe_4 in Fe_4 @SWNT and Fe_4 @N-SWNT compared with that in pure SWNT. The vacuum level is aligned at 0 eV. The red and blue regions in plot II and III indicate a charge increase and decrease, respectively. f) Schematic illustration of the concept of “chainmail for catalyst.” a) Reproduced with permission.^[14] Copyright 2016, Nature Publishing Group. b,c,e) Reproduced with permission.^[13] Copyright 2013, Wiley-VCH. d) Reproduced under the terms of the CC-BY Creative Commons Attribution 3.0 Unported Licence.^[16] Copyright 2015, Royal Society of Chemistry.

the catalytic activity of nonprecious-metal catalysts will not be shielded by the graphene shells.

2.2. Modulation and Optimization toward the TM@Graphene Chainmail Catalyst

The structural modulation of a material usually has an important effect on its electronic properties and thereby the corresponding catalytic performance. Therefore, a structural and electronic modulation and optimization of this unique chainmail catalyst will promote it to make the most of its advantage for the catalytic reactions under harsh conditions. Various factors can influence the electron penetration process from TMs through graphene shell, such as thickness of graphene shell, heteroatom doping within graphene surface, TM type, size, curvature of graphene shell, etc. (Figure 2a). Recently, a number of important studies have been carried out by considering these factors to achieve the modulation and optimization in the TM@graphene chainmail catalysts.

First, the layer number of graphene shell in the chainmail catalyst is often changeable during the preparation, and the effect of the graphene layer thickness on the electron transfer should be considered. Several studies have shown that the

electron shuttle across the graphene layer is limited to no more than three to four carbon layers,^[47,48] which indicates that reducing the graphene layer number of the shell will reinforce such an electron transfer process. Lately Deng et al. found that graphene layer number decrease will significantly promote the electron transfer from TMs to graphene shell, which therefore enhances the O_2 adsorption on the graphene surface and subsequently the oxygen reduction catalytic activity, according to both the experiments and theoretical calculations (Figure 2b).^[45] More recently, only one to three layers graphene encapsulating CoNi catalyst (Figure 2c)^[46] and single-layer graphene encapsulating FeNi catalyst^[49] both showed high activities toward hydrogen production and oxygen evolution separately in electrocatalytic water splitting. It can be attributed to the greatly enhanced electron penetration through the graphene layer to tune the electronic structure of the graphene surface (Figure 2d).^[46] The conducted studies indicate the thinner the graphene shell, the more the electron transfer and the higher the catalytic activity.

The heteroatom doping (e.g., N, B, and P) has been proved as an effective way to tune the electronic properties and catalytic performance of graphene through electron interaction.^[37,38,50–53] So the introduction of heteroatoms into the graphene shell will affect the electron transfer from TMs and the

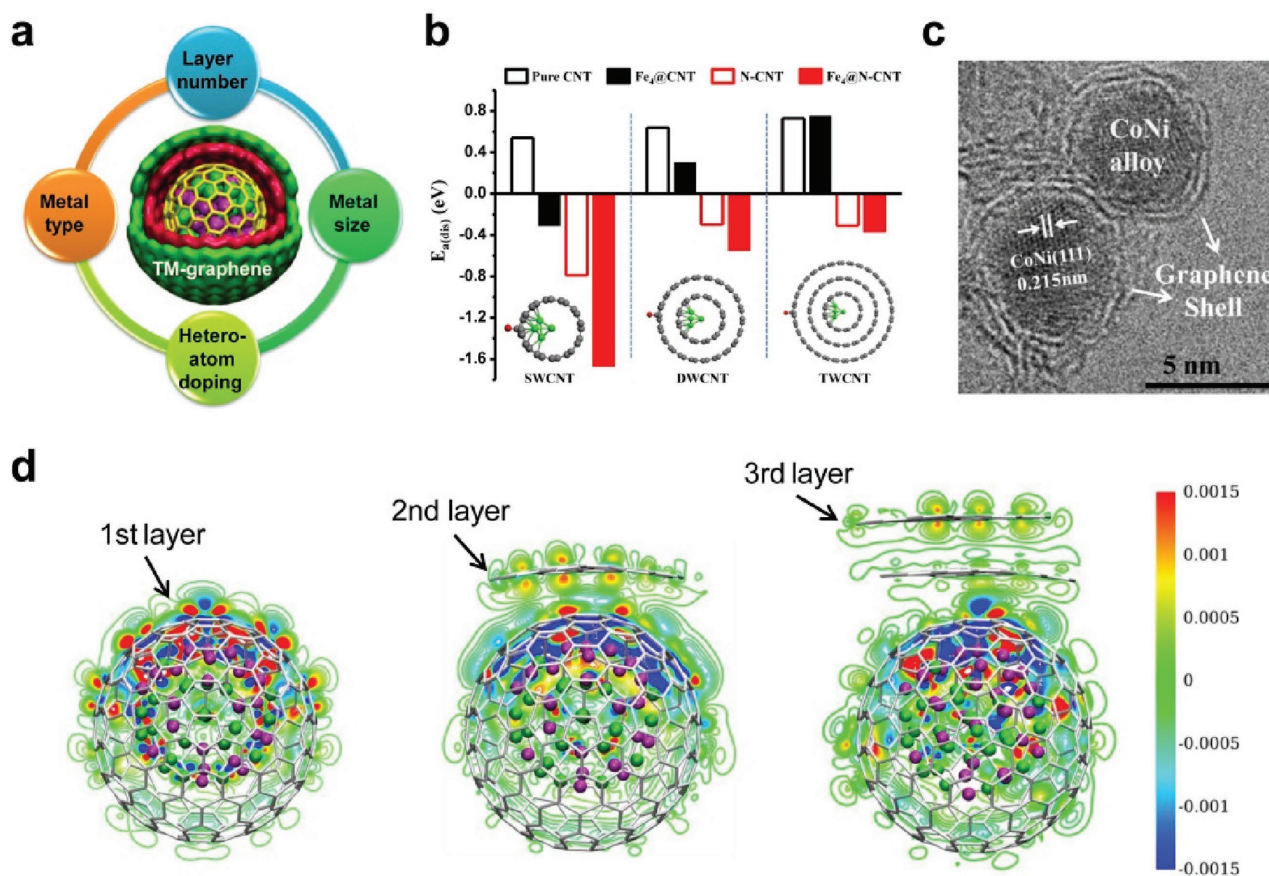


Figure 2. a) Schematic illustration of the structural and electronic modulation within the TM-graphene chainmail catalyst. b) The DFT calculated dissociative adsorption energy of O_2 ($E_{a(dis)}$) on the carbon surface of pure or N-doped (doped with two nitrogen atoms) SWCNTs, DWCNTs, and TWCNTs with or without an enclosed Fe_4 cluster. c) HRTEM image of graphene shell encapsulating CoNi nanoparticles (CoNi@NC). d) The redistribution of electron density after a CoNi cluster is covered by one to three layers of graphene. The red and blue regions represent increased and decreased electron density, respectively. b) Reproduced with permission.^[45] Copyright 2013, Royal Society of Chemistry. c,d) Reproduced with permission.^[46] Copyright 2015, Wiley-VCH.

corresponding catalytic activity of the graphene shell surface. For example, when N atoms were doped into the graphene shells, the electrocatalytic oxygen reduction and hydrogen evolution processes can be both promoted by using such kind of chainmail catalysts. It was because the presence of N dopants in the graphene shell will further increase the DOS near the Fermi level according to the density functional theory (DFT) calculations.^[13,45,46,54] Furthermore, Zhang et al. recently co-doped B and N atoms into the graphene cages that encapsulating Co nanoparticles. They found that the co-doping of B and N atoms can produce a synergistic effect in tuning the electronic properties of the surface carbon atoms, as well as can couple with the encapsulated Co nanoparticles to promote the electrocatalytic hydrogen evolution activity.^[55] In addition, Ryu et al. described a new type of carbon shell coating Co nanoparticles, of which the surface composites are modified by P incorporation. This P-doped catalyst exhibits efficient oxygen electrode catalytic activity.^[56]

Different metals possess different work functions, leading to the difficulty and number of electron transfer from TMs to graphene shell to be different. The surface electronic properties and local work function of graphene can be effectively tuned

through altering the TM types, which therefore optimizes the catalytic performance in a specific reaction system. For example, Deng et al. found that metallic Co encapsulated inside the graphene shell will show much higher modulation ability to the hydrogen evolution activity of graphene than that of metallic Fe.^[54] Xing et al. gained a better counter electrode (CE) toward I_3^-/I^- reduction reaction with encapsulating Ni nanoparticles in comparison to the Co nanoparticles.^[57] In addition, when graphene shell is used to encapsulate TMs, the graphene matrix will become curly. The electron transfer process and the electron distribution on the graphene surface may be affected by the curvature of graphene shell and the particle size of TMs. Such effect still needs a detailed and deep study from experiments and theoretical calculations.

3. Expansion of the Chainmail Concept into More TM@2D Crystal Catalysts

The chainmail catalyst can be employed in some reaction systems under harsh conditions, where bare nonprecious-metal catalysts usually appeared unstable. Such advantage of the

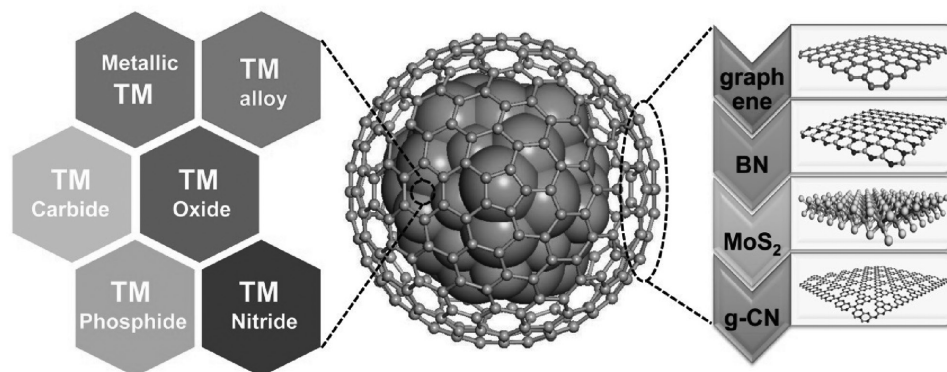


Figure 3. Schematic illustration of the different TM materials and 2D crystal shells within the chainmail catalyst.

chainmail catalyst has been referenced by more researchers. Based on the fact that both TM materials and 2D crystals possess abundant alternatives, flexible combination between different TM materials and 2D materials can be achieved. Recently, diverse TM materials and 2D crystal shells have been fabricated and studied (Figure 3), which enriched such class of chainmail catalysts and enormously expanded their applications (Table 1).

3.1. Variation of the TM Types

In the initial introduction of chainmail catalyst, metallic TMs were encapsulated into the graphene shells as electron donor, such as Fe, Co, Ni, or their alloy nanoparticles. Science then, many kinds of TM materials have been successfully encapsulated for various catalytic processes, such as TM carbide, TM oxide, TM phosphide, TM nitride, etc. (Figure 3).

When TM carbide was encapsulated in graphene shell, the electronic modification on graphene surface to promote catalytic activity can also be found. For example, Chen et al. prepared a Co_xC encapsulated in carbon shell catalyst, showing high oxygen reduction activity which is comparable with that of 20 wt% Pt/C in 0.1 M KOH electrolyte. It also exhibited a high activity in 0.1 M HClO_4 with a near-complete $4e^-$ pathway.^[58] In addition, when Co_3ZnC and Co were simultaneously encapsulated in graphene layers, the heterostructure of $\text{Co}_3\text{ZnC}/\text{Co}$ will synergistically enhance the adsorption of reaction intermediates to be beneficial to the electrocatalytic activities on carbon surface. The material ultimately served as a high bifunctional oxygen catalyst toward oxygen reduction and oxygen evolution processes.^[59]

Besides TM carbide, TM oxide has also been encapsulated into the graphene shell to form the unique chainmail catalyst. In the report of Li et al.,^[60] the presence of CoMnO nanoparticles inside graphene framework will contribute to the decrease of local work function via the electron transfer on graphene surface to promote the catalytic activity. It can be served as an efficient bifunctional water-splitting electrocatalyst. Furthermore, combining with a silicon photovoltaic cell, this bifunctional catalyst enabled unassisted solar water splitting with a solar-to-hydrogen conversion efficiency of 8.0%. In addition, Cheng et al. reported a MnO nanoparticles encapsulated in mesoporous few-layer carbon (MnO@FLC), which shows

excellent oxygen reduction activity with an onset potential of -0.005 V and a half-wave potential of -0.153 V (vs Ag/AgCl). They disclose that the few-layer carbon could be activated by the encapsulated MnO nanoparticles and further become active sites for the oxygen reduction process.^[61]

Recently, TM phosphide has attracted much attention in the electrocatalysis fields due to the high performance,^[62–64] but the instability in harsh environment is still existed. Zhuang et al. developed a one-pot strategy for the fabrication of Co_2P encapsulated in N, P-doped graphene ($\text{Co}_2\text{P@NPG}$) and used it as an electrocatalyst for hydrogen production under strong acidic or alkaline medium.^[65] Owing to the synergistic modulation effect of Co_2P nanoparticles and N, P dopants, a high hydrogen evolution activity was obtained. Meanwhile, encapsulation by graphene effectively prevent nanoparticles from corrosion, exhibiting nearly unfading catalytic performance during 30 h testing. Moreover, this method is versatile and can be easily extended to other TM phosphides such as Fe_2P , Ni_2P , and Pd_5P_2 encapsulated in graphene shells.

Similarly, when Fe_2N was encapsulated in the carbon shell, it showed outperformed activity than Pt toward oxygen reduction reaction in alkaline electrolyte and comparable activity to Pt/C (onset potential of 0.82 V versus 0.91 V) in acidic electrolyte. It also showed outstanding durability and resistance to methanol crossover, ascribed to that the carbon shell suppresses the dissolution or agglomeration of Fe_2N nanoparticles.^[66] On this basis, dual TM compounds can be embedded into graphene shells, providing a hybrid Co_2P and Co_xN nanoparticles encapsulated in N-doped graphene shell catalyst. The positive synergistic effect of the coexistence of Co_2P and Co_xN as well as their strong coupling with graphene greatly promote the electron transfer between the catalyst surface and reaction molecules, which eventually bring the optimized structure as an efficient bifunctional catalyst in the rechargeable Zn–air batteries.^[67]

3.2. Variation of the 2D Materials

The successful research of graphene has promoted other 2D crystal materials (BN, MoS_2 , etc.) to be prepared and studied.^[68–72] Like graphene, they also can be adopted to encapsulate the TM materials due to their bendable plane structure, though the experimental construction is still remained

as a challenge compared to the graphene. Recently, there have been a few studies on nongraphene shells covering TM catalysts, such as BN, MoS₂, graphitic carbon nitride (g-CN), etc. (Figure 3).

BN, a typical chemical inert 2D crystal, usually cannot act as an efficient catalyst. However, when it was covered on metallic Ni surface, the catalytic activity toward oxygen reduction reaction can be achieved according to the DFT calculations. The studies showed that the mixing between the metal d and BN π bonds will provide the electron transport to the active sites on BN, promoting the adsorption of O species such as O₂, OOH, OH, and O. Therefore, the BN can be functionalized by the underneath metal Ni to become catalytically active. On the basis of this calculated results, one can further tune the catalytic activity of BN by choosing a suitable TM.^[73] Encouragingly, Uosaki et al. have demonstrated the validity of this BN covering TM catalyst from experiment accompanied with DFT calculations. In their experimental results, BN nanosheets supported on Au (111) electrode will significantly reduce the overpotential for oxygen reduction reaction compared with pure Au (111) electrode and BN nanosheets on bare glassy carbon electrode. DFT calculations show that a slight increase of DOS near the Fermi level is observed when BN supported on Au (111) through the BN–Au interaction. It promotes the O₂ adsorption on BN and thereby induces the catalytic activity on the inert BN surface.^[74]

Another 2D crystal material MoS₂ has attracted great research interest during recent years, but no effective experimental method yet can be used to achieve the structure of MoS₂ covering TMs, except for theoretical studies. Chen et al. investigated the electronic and chemical properties of a single-layer MoS₂ attached on different TM substrates such as Ir (111), Pd (111), and Ru (0001). Their DFT calculations indicated that by using hydrogen adsorption as a testing example, the chemical reactivity of the absorbed MoS₂ layer can be substantially altered by the introduction of metal substrate. An electron transfer from the metal to the MoS₂ layer will enable a stronger H–S coupling for enhancing the hydrogen binding by as much as ≈ 0.4 eV, which thereby can boost the hydrogen production and related chemical process.^[75]

g-CN, another important carbon-based 2D crystal material, owns a similar 2D structure to that of graphene and has been widely studied when directly used as catalyst.^[76,77] When using g-CN to encapsulate the TMs, it may further enhance the intrinsic activity due to the additional electronic contribution from the TMs. One typical example is come from Ding and co-workers,^[78] by using carbon nitride (CN) encapsulating Ni as the catalyst to promote hydrogenation of nitrobenzene to produce *p*-aminophenol in strong H₂SO₄ (1.5 M). They found that it showed a high activity and stability, while for this reaction only precious metals can be used in previous studies due to the strong corrosion of H₂SO₄. The characterization demonstrated that metallic Ni donates electrons to CN, promoting the hydrogen directly to be absorbed and activated on the CN surface for reaction with nitro compounds to amino compounds. The direct contact of the metal with the harsh environment is avoided, which makes it highly stable. Dai et al. have also embedded metallic Co into nitrogen-rich carbon nitride (Co@NCN). The metallic Co nanoparticles are well-confined and

protected by the NCN to exhibit excellent stability (5000 cycles) in acidic hydrogen evolution reaction. The electronic coupling between Co nanoparticle and NCN shell accelerates the charge transfer to provide outstanding activity with an onset potential of -89 mV versus RHE.^[79]

Besides the metallic TMs, other TM compounds can also be encapsulated into g-CN shells, such as TM oxide and TM carbide. Mahmood et al. have reported an in situ solvothermal synthesis to fabricate C₂N 2D network encapsulating Co oxide (Co@C₂N) structure. The obtained catalyst exhibited outstanding catalytic activities for hydrogen generation from the hydrolysis of alkaline sodium borohydride (NaBH₄) solutions. The rate of maximum hydrogen production is comparable to the best reported values for other precious-metal catalysts in alkaline solutions. The high catalytic activity may originate from the strong interaction between the Co oxide nanoparticle and the C₂N framework.^[80] In addition, Liu et al. recently prepared nanosized Fe₃C encapsulated within mesoporous carbon nitride (Fe₃C@mCN), exhibiting a superior oxygen reduction activity and much better durability compared to that of commercial Pt/C catalyst.^[81]

4. Application

In view of the advantages in such chainmail catalysts (TM@2D crystal), many reaction processes under harsh conditions (e.g., strong acidic or alkaline medium, corrosive solution, high overpotential, and high temperature) can employ them to enhance the stability of TM catalysts. In recent years, the applied reaction systems of the chainmail catalysts have been extended into several important research fields, including the fuel cells, water splitting, CO₂ conversion, solar cells, metal–air batteries and heterogeneous catalysis (Table 1), showing great potential of the unique chainmail catalysts for catalysis.

4.1. Oxygen Reduction Reaction (ORR)

Fuel cells have been regarded as promising clean and efficient energy conversion devices, in which the sluggish reaction kinetic of the ORR at cathode is the major limit to increase the energy conversion efficiency. Considering both the high catalytic performance and easy to be commercialized, nonprecious alternatives should be developed to replace Pt-based precious electrocatalysts in order to reduce the cost of this device. Especially, the instability of nonprecious-metal catalysts under working conditions (strong acid or base, high overpotential) and poison environment (e.g., CO, SO₂, and CH₃OH) has to be overcome. The unique chainmail catalyst showed the possibility to become the Pt-alternative electrocatalyst,^[61,82–109] which was first tried by Deng et al. (Figure 4a). In their study, metallic Fe nanoparticles were encapsulated by graphene shell, exhibiting both high activity (Figure 4b) and high durability (Figure 4c). The reason for the performance enhancement is as discussed in the concept origin section that a part of the electron will transfer from the Fe to the graphene surface. It leads to the decrease of local work function on graphene surface, which further increases the DOS near Fermi level of graphene and

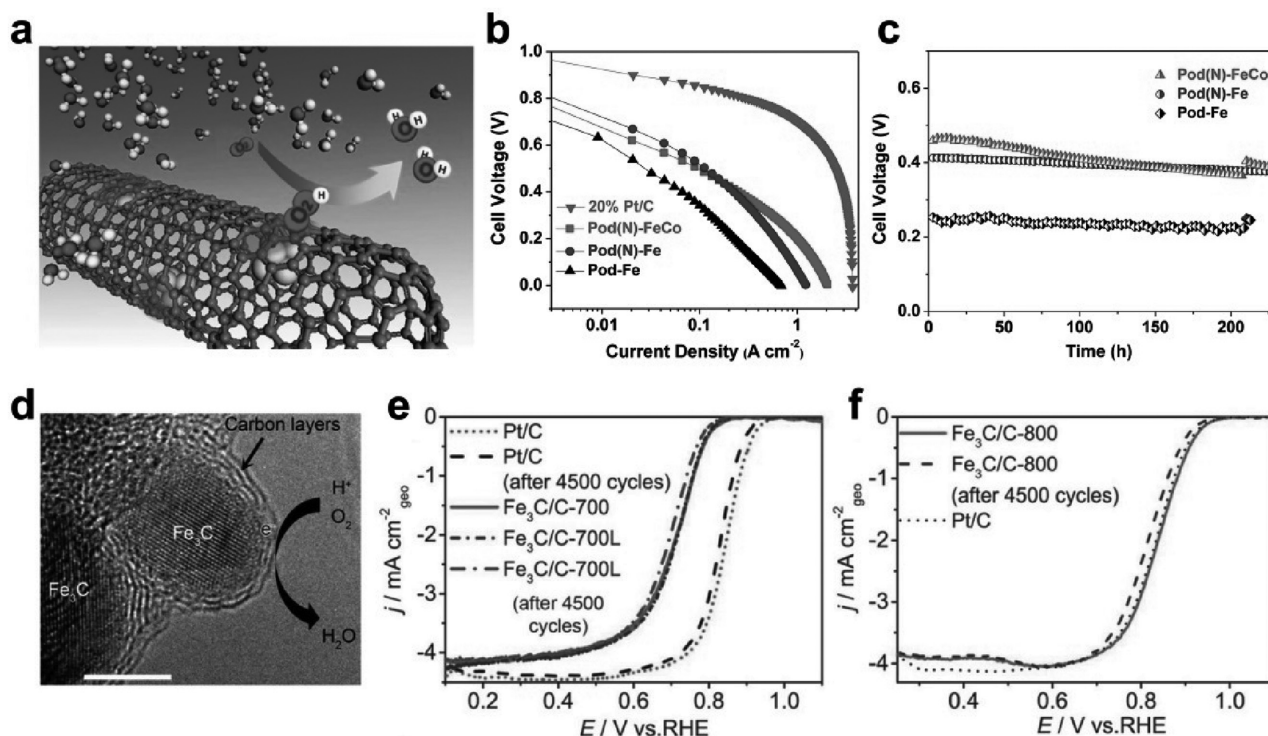


Figure 4. a) A scheme of the reaction process for ORR at the surface of $\text{Fe}_4\text{@SWNT}$. b) A single $\text{H}_2\text{-O}_2$ fuel cell performance test with Pod-Fe, Pod(N)-Fe, Pod(N)-FeCo, and commercial 20% Pt/C (JM) cathodes. c) $\text{H}_2\text{-O}_2$ fuel cell durability test with the Pod-Fe, Pod(N)-Fe, Pod(N)-FeCo cathodes at a steady current of 0.1, 0.5 and 0.5 A, respectively. d) Oxygen reduction process on $\text{Fe}_3\text{C/C-700}$ (scale bar = 5.00 nm). e) LSVs of $\text{Fe}_3\text{C/C-700}$, $\text{Fe}_3\text{C/C-700L}$, and Pt/C at 900 rpm in O_2 -saturated 0.1 M HClO_4 before and after 4500 potential cycles. f) LSVs of $\text{Fe}_3\text{C/C-800}$ and Pt/C at 900 rpm in O_2 -saturated 0.1 M KOH before and after 4500 potential cycles. a–c) Reproduced with permission.^[13] Copyright 2013, Wiley-VCH. d–f) Reproduced with permission.^[110] Copyright 2014, Wiley-VCH.

therefore promotes the oxygen adsorption on graphene surface to enhance the catalytic activity.^[13]

Afterward, more metallic TMs were successfully introduced into the graphene shell for the ORR, owing to the progress in the understanding of material preparation and experimental technology. For example, Liu et al. have devised a facile and cost-effective solid-state thermal reaction of cyanamide and transition-metal chloride to prepare TM nanoparticles (Fe, Co, and Ni) encapsulated in N-doped graphene shell. The different TMs showed different promotion to the ORR activity, where the Co enclosed in the N-doped carbon even owned a higher activity in terms of the half-wave potential value (0.84 V) compared to commercial Pt/C catalyst (0.82 V) as well as a better durability under the long-term stability and methanol-tolerance measurements.^[111] Likewise, Kong et al. prepared the nitrogen-doped carbon cubes embedded with numerous metallic Co nanoparticles by one-step pyrolysis of a unique “cage-in-cage” Co metal-organic framework (MOF). With about 60 wt% Co particles in the prepared sample, the obtained catalyst shows high electrocatalytic activity for the ORR. The efficiency is comparable to the commercial Pt/C catalyst, and the durability and methanol-tolerance performance are better than commercial Pt/C catalyst.^[112]

Besides the metallic TM nanoparticles, TM carbides are often encapsulated due to their similar and facile prepared process as the metallic TMs. For example, the Fe_3C -based electrocatalysts have been often reported in the literature.^[113,114] Hu et al.

encapsulated Fe_3C nanoparticles in graphitic layers (Figure 4d), which was highly active and stable toward oxygen reduction reaction in both acidic and alkaline electrolytes (Figure 4e,f).^[110] In their catalytic nature study, the fact that Fe_3C nanoparticles activated the surrounding graphene shell to make the outer surface of the carbon layer active toward oxygen molecules is the reason why this $\text{Fe}_3\text{C/C}$ catalyst exhibit excellent electrocatalytic performance (Figure 4d).

Guo's group has done several interesting works by encapsulating Fe_3C nanoparticles to catalyze the ORR. For example, they demonstrated a new one-step soft-template-induced strategy through annealing a mixture of PEG-PPG-PEG Pluronic P123, melamine and $\text{Fe}(\text{NO}_3)_3$ at high temperature, for controlled synthesis of Fe_3C encapsulated in graphene. The resulting hybrid electrocatalysts showed a high ORR activity with a half-wave potential of 0.861 V (vs RHE) which is much more positive than that of 20% Pt/C (0.812 V vs RHE) in 0.1 M KOH solution, and a comparable onset potential to that of Pt/C catalyst in acidic media. More importantly, the as-prepared electrocatalysts exhibited much better durability than the commercial Pt/C catalyst in both alkaline and acidic solutions.^[115] On this basis, they developed a simple method to achieve manufacturing hierarchical micro-, meso-, and macropores on the walls of graphene to introduce a 3D diffusion pathway for O_2 and electrolyte. This method can also bring more electrochemically active and stable Fe_3C nanoparticles into the graphene shell for increasing the active domains. Through these two important

features, the modified catalyst exhibits a higher ORR activity and superior durability relative to previous unhandled ones and commercial Pt/C catalyst in both acidic and alkaline media.^[116]

Since the hierarchical modulation within the chainmail catalyst can synergistically boost the ORR process, some studies focus on the design and synthesis of 3D hybrid framework catalyst to achieve the activity enhancement. Zhang et al. employed a simple NaCl-assisted pyrolysis approach for the in situ synthesis of 3D hybrid of metallic Fe and Fe₃C encapsulated in graphitic carbon integrating with carbon nanosheets. The obtained sample preserved the intrinsic catalytic centers of graphene enclosing metallic Fe/Fe₃C nanoparticle, and additionally possessed enlarge specific surface area and porosity for accommodating sufficient active sites and facilitating electron/mass transfer due to the structural advantage of this 3D carbon hybrid. Benefiting from these features, the developed hybrid exhibited a significantly enhanced electrocatalytic activity and durability for the ORR. Another important advantage is that NaCl can be easily recycled via a recrystallization process, which makes the preparation cost-effective and easily scalable.^[117] In addition, Hou et al. also prepared a 3D nanoarchitecture comprising CoNi alloy encapsulated in N-doped graphene grown on N-doped porous carbon nanosheets with the desirable porosity, sufficient active sites and good conductive networks. When evaluated as an electrocatalyst for ORR, the hybrid shows efficient catalytic activity, high selectivity, superior durability, and strong tolerance against methanol crossover compared with the commercial Pt/C catalyst, which are even better than those of most previous reported carbon-based electrocatalysts.^[118]

In view of the graphene layer thickness being very important in affecting the electron transfer between the TMs and graphene shell, controlling the layer thickness is also a significant research direction. Noh et al. recently optimized the shell thickness by oxidizing carbon with CO₂ at high temperature within the framework of Cu particles encapsulated by N-doped carbon (Cu@N-C). The Cu@N-C catalyst after CO₂ treatment showed a dramatically enhanced ORR activity to a similar level to Pt/C catalyst, and a better stability than Pt/C catalyst under long-time tests. Their DFT calculations displayed that the encapsulated Cu particle donates electronic charges to the N-C layers, which enables favorable electronic interactions between the carbon surface and adsorbed molecules in the ORR to contribute the high activity.^[119]

4.2. Hydrogen Evolution Reaction (HER)

Hydrogen as a clean and renewable fuel has long been expected to replace the traditional fossil fuels to act as potential energy carrier for future energy infrastructure. The most abundant and renewable hydrogen source is from the water, which makes the electrocatalytic water splitting become an important high-efficient technology for the hydrogen production. One half-reaction in water splitting is the HER, which consumes Pt-based precious metals as the state-of-the-art catalysts. However, the high cost and limited reserve of Pt-based electrocatalysts require seeking for highly active and stable nonprecious-metal catalysts, which usually suffer from leaching or corrosion in strong acidic or alkaline electrolyte. The chainmail catalyst

has been originally applied into the HER system by our group (Figure 5a) and Asefa's group recently.^[120–137]

Our experiments and DFT calculations indicated that the adsorption of hydrogen on pristine graphene is too weak because the chemically inert surface of graphene leads to the adsorption process thermodynamically unfavored. Thus, graphene shows poor HER activity. After graphene encapsulating TM nanoparticles, the electron will transfer from TMs to graphene due to the lower work function of TMs compared with graphene. It significantly modified the electronic state near the Fermi level of carbon atoms to make the band center of the occupied states of the C–H bond locate in a lower energy regime, which means a stronger chemical bonding between hydrogen atom and carbon atom to enhance the hydrogen adsorption on the graphene surface (Figure 5b) and thereby the HER activity (Figure 5c). Meanwhile, the stability of nonprecious-metal catalysts is significantly enhanced with the protection of graphene shell.^[54]

Almost at the same time, Asefa's group also reported a simple, easily scalable synthetic route involving thermal treating of TM cations and graphitic carbon nitride to prepare TM-embedded N-rich graphene shell. The material is proven to be highly efficient for HER.^[139] They thought the encapsulated metal nanoparticles can result in the decreased local work function on carbon surface through the facile electron transfer from metal particles to graphene. It will also couple with the N dopants to favor the hydrogen adsorption and thereby the catalytic activity. The results of the electrocatalytic measurements of different enclosed TMs showed the activity increase in an order of Fe < Ni < Co in their studies, which is consistent with the results of our study showing the modulation ability as the sequence of Fe < Co (Figure 5c).

In consideration of the Co atom in the chainmail catalyst is a much better choice for the HER system, many studies have selected it as the encapsulated materials. For example, Zhou et al. adopted a facile solvothermal and subsequent high-temperature calcination procedure by decomposition of cyanamide and concurrent reduction of Co²⁺ to prepare N-doped carbon wrapping Co nanoparticles on N-doped graphene nanosheets (Co@NC/NG) for HER.^[140] The resulting composites were found to possess high conductivity and abundant active sites, leading to the Co@NC/NG hybrids exhibited a remarkable electrocatalytic activity with an onset potential at only –49 mV (vs RHE) and excellent catalytic stability. They also conducted the DFT calculations to unravel the fundamental mechanism by using a C₆₀ molecule with a Co atom in it to simulate the carbon-wrapping Co nanoparticles in the experiments. It was found that about 0.7 electron was transferred from Co to the nearby carbon atoms raising the Fermi level, and some energy levels in the highest occupied molecular orbital (HOMO)–lowest unoccupied molecular orbital (LUMO) gap of the pure carbon cage were introduced. These were expected to decrease the local work function and increase chemical reactivity, leading to HER activity enhancement, as observed experimentally. In addition, Su et al. demonstrated a straightforward method to prepare highly integrated Co-nanoparticle-rich carbon nanofibers via self-assembly and carbonization of metal-organic complex nanofibers, possessing high contents of well dispersed Co nanoparticles estimated to be 51.3 wt%. The as-obtained

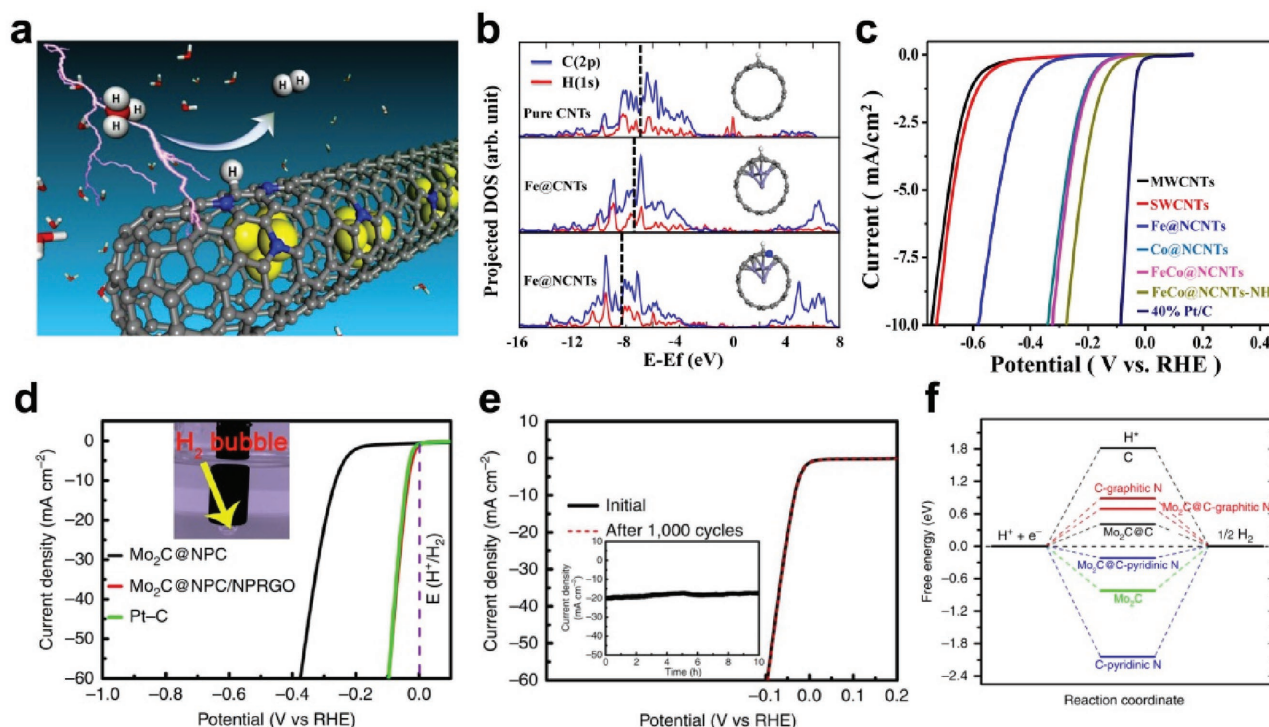


Figure 5. a) A schematic representation of the HER process on the surface of Fe@NCNTs. b) Comparison of projected density of states (DOS) of H(1s) and its bonded C(2p) when H is adsorbed on the surface of pristine CNTs, Fe@CNTs, and Fe@NCNTs. The dashed lines present the center of the occupied band. c) Polarization curves of Fe@NCNTs, Co@NCNTs, FeCo@NCNTs, FeCo@NCNTs-NH along with MWCNTs, SWCNTs, and 40% Pt/C for comparison. d) Polarization curves of Mo₂C@NPC, Mo₂C@NPC/NPRGO, and Pt-C (inset: the production of H₂ bubbles on the surface of Mo₂C@NPC/NPRGO). e) Polarization curves of Mo₂C@NPC/NPRGO initially and after 1000 CV cycles. Inset: Time-dependent current density curve of Mo₂C@NPC/NPRGO under a static overpotential of 48 mV for 10 h. f) Calculated free-energy diagram for HER on various studied system. a–c) Reproduced with permission.^[54] Copyright 2014, Royal Society of Chemistry. d–f) Reproduced under the terms of the CC-BY Creative Commons Attribution 4.0 International License.^[138] Copyright 2016, Nature Publishing Group.

catalyst exhibited superior HER stability and activity with an overpotential of only 196 mV (vs RHE) at the current density of 10 mA cm⁻² in 1 M KOH and surpassed the HER performance of benchmarked Pt/C in concentrated alkali solution.^[141]

Besides the nonprecious TMs (Fe, Co, Ni, etc.), other precious TMs like Au can also be encapsulated as HER catalyst although Au nanoparticle itself is rare seen to be efficient for HER studies. In addition, the uptake of precious metals from electronic waste and subsequently manufacturing as catalyst is of environmental significance and potential commercial value. Recently, Zhou et al. prepared evenly dispersed Au nanoparticles (≈20 nm) embedded in N-doped carbon (Au@NC) after bioreduction of precious metals by microorganism cells. The high resolution transmission electron microscopy (HRTEM) images and XPS results confirm the strong interaction generated by the in situ bioreduction and calcination process. It was advantageous for the charge transport between the Au and N-doped carbon to modulate the electronic density states of N-doped carbon and to promote the catalytic activity. The optimized Au@NC catalyst displays efficient HER activity with a small onset potential of only -54.1 mV (vs RHE), a Tafel slope of 76.8 mV dec⁻¹, a large catalytic current density, and electrochemical durability, while the bare Au nanoparticles or supported on N-doped carbon both showed a negligible HER activity.^[142]

As a result of the similar d-band electronic DOS to that of Pt and high electrical conductivity, TM carbides, especially molybdenum carbide, had long been expected to be promising non-Pt HER electrocatalysts.^[143,144] However, the problems of inevitable aggregation and/or excessive growth of molybdenum carbide nanoparticles and the ready oxidation of the surface of molybdenum carbide nanoparticles to molybdenum oxide species still remained. Recently, these disadvantages have been overcome by fabricating the chainmail catalyst, i.e., encapsulating the molybdenum carbide nanoparticles into the graphene shells. One report was from Zou and co-workers.^[145] They adopted a simple one-step thermal treatment of homogeneously mixed ammonium molybdate and dicyandiamide in Ar atmosphere to produce ultrasmall molybdenum carbide (Mo₂C) nanoparticles embedded in nitrogen-rich carbon (NC) nanolayers (Mo₂C@NC). The Mo₂C@NC hybrid nanoelectrocatalyst shows remarkable catalytic activity, great durability, and about 100% Faradaic yield toward the HER over a wide pH range (pH 0–14). More importantly, it owns even a much higher catalytic activity than the bare Mo₂C. The DFT calculations indicated the presence of the synergy between Mo₂C and N dopants to the neighboring C atoms through the electron transfer process can tune the hydrogen adsorption on Mo₂C@NC to a moderate level instead of too weak on pristine graphene and too strong on bare Mo₂C, resulting in the final high HER activity. Ma et al.

used the similar method by heating the mixture of dicyanamide and ammonium molybdate to synthesize the ultrafine Mo₂C nanoparticles uniformly embedded in a carbon matrix. It showed superior HER activity in acidic media, with a very low onset potential of -6 mV, a small Tafel slope of 41 mV dec⁻¹, and a large exchange current density of 0.179 mA cm⁻², as well as a good stability during operation for 12 h. They also considered that the ultrathin graphene shells could promote electron penetration from the Mo₂C to the graphene surface to improve reactivity for HER.^[146]

In addition, for the purpose of preventing Mo₂C nanoparticles from aggregating and increasing the dispersion of active sites, Li et al. further coupled Mo₂C encapsulated by N,P-co-doped carbon shells with N,P-co-doped reduced graphene oxide (Mo₂C@NPC/NPRGO) using a PMo₁₂ (H₃PMo₁₂O₄₀)-PPy/RGO nanocomposite as the precursor.^[138] The obtained composites possessed a unique structure with the Mo₂C@NPC and NPRGO highly dispersed and strong conjugated, which is favorable for the fast mass transport of reactants and facilitates the electron transfer. After the structural optimization, the catalyst exhibits excellent electrocatalytic activity for the HER, with a low onset potential of 0 mV (vs RHE) and an overpotential of only ≈34 mV (vs RHE) to achieve a current density of 10 mA cm⁻² (Figure 5d), a small Tafel slope of 33.6 mV dec⁻¹, and excellent stability in acidic media (Figure 5e). The HER catalytic activity, comparable to that of commercial Pt/C catalyst, is even superior to those of the best reported nonprecious-metal

catalysts. Their DFT calculations also demonstrated that the synergistic effect between Mo₂C and heteroatom dopants contributes to the excellent HER activity (Figure 5f).

4.3. Oxygen Evolution Reaction (OER)

In the water splitting process, besides the HER half-reaction to directly produce hydrogen, the other important half-reaction, known as OER, is usually kinetically sluggish and largely hinders the overall efficiency of water splitting. Currently, precious-metal-based catalysts including RuO₂, IrO₂, etc. can efficiently reduce the energy barrier and thus increase the OER efficiency, but their large-scale commercialization is still hindered by the limitations of their scarcity and high cost. Search for nonprecious-metal catalysts as alternatives to the OER electrocatalysts also proceeded in this oxygen electrode. However, low efficiency and instability of nonprecious-metal catalysts still remain when they suffer long-time operation or accelerated degradation measurements under strong acidic/alkaline electrolytes.^[147–149]

To this end, Cui et al. recently applied the chainmail catalyst into the OER system (Figure 6a).^[49] They devised a universal strategy to directly synthesize single-layer graphene encapsulating uniform earth-abundant 3d TM nanoparticles, such as Fe, Co, Ni and their alloys assisted by the channel of mesoporous silica (Figure 6b). Electrochemical measurements showed that the single-layer graphene encapsulating metals

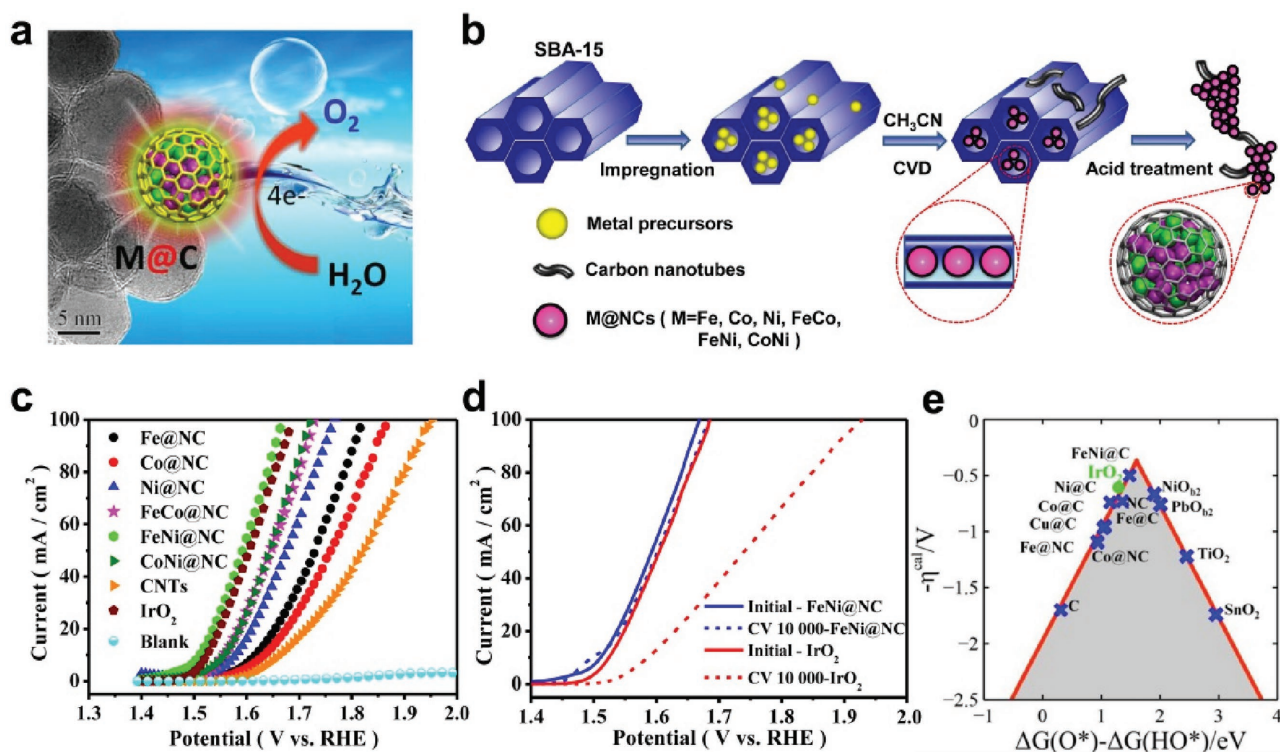


Figure 6. a) A schematic representation of the OER process on the surface of graphene encapsulating metal catalyst. b) Schematic illustration of the synthesis process of M@NCs from metal-containing precursors and SBA-15. c) OER polarization curves for M@NCs in comparison with CNTs and IrO₂ with the same mass loading. d) Durability test of FeNi@NC in an alkaline electrolyte in contrast to IrO₂. e) The calculated negative overpotential (η^{cal}) against the universal descriptor $\Delta G(\text{O}^*) - \Delta G(\text{HO}^*)$ on different catalysts. a–e) Reproduced with permission.^[49] Copyright 2016, Royal Society of Chemistry.

exhibited an OER activity as the order of $\text{Co} < \text{Fe} < \text{Ni}$. The optimized FeNi alloy catalyst showed the best activity with only 280 mV overpotential at current density of 10 mA cm^{-2} (Figure 6c) and a high durability without degradation even after 10 000 cycles (Figure 6d), both of which are superior to those exhibited by commercial IrO_2 . DFT calculations indicated that the single-layer graphene immensely promoted the electron transfer from the encapsulated metals to the graphene surface, which optimizes the electronic structure of the graphene surface and further tunes the binding energies of reaction intermediates (O^* and HO^*) on the graphene surface. By changing the type of metal, the OER descriptor that the free energy of O^* relative to HO^* ($\Delta G(\text{O}^*) - \Delta G(\text{HO}^*)$) can be adjusted to an optimal value and thereby the OER activity can be highest triggered on the inert graphene surface (Figure 6e).

Furthermore, Xia et al. also synthesized a hollow framework constructed from interconnected carbon-encasing Co nanoparticles and N-doped carbon nanotubes starting with ZIF-67 particles as single precursor. It performed as an efficient and stable electrocatalyst for OER with a current density of 10 mA cm^{-2} at a potential of 1.60 V (vs RHE), comparing favorably to other reported nanocarbon-based catalysts and IrO_2/C catalyst. The remarkable electrocatalytic properties are mainly attributed to the synergistic effect between the unique TM-carbon composite and the robust hollow structure.^[150]

The two half-reactions of OER and HER processes both require efficient catalysts to reduce the energy barrier and further accelerate the overall water splitting. The development of bifunctional electrocatalysts with high activities toward both the OER and HER in the same electrolyte could be a promising way, as it may simplify the requirement for diverse equipments and processes. In consideration of this unique chainmail catalyst can catalyze both the anodic and cathodic reactions of water splitting efficiently, it could be a good choice for promoting the electrochemical processes. For example, Zhang et al. prepared metallic Ni-Fe alloy nanoparticles encapsulated in carbon shell by pyrolyzing a precursor composed of Ni and Fe salts with urea under inert argon atmospheres without any post-treatments. The metal ratios in the nanoparticles can be easily altered, and the amount of Fe was found to have a significant influence on both the HER and OER activities of the catalysts. For the OER, the best activity was achieved with 10 at% Fe in the metal alloy. However, for HER, the activity decreased with increasing the Fe contents. When it was integrated into symmetric two-electrode water-splitting cells, the catalyst with 10 at% Fe (with a mass loading of 2 mg cm^{-2} on Ni foam for both the cathode and anode) could achieve a current density of 10 mA cm^{-2} with a voltage of only 1.58 V and show negligible degradation after 24 h of operation.^[151]

In addition, an electrospinning technique was adopted by Zhao et al. to synthesize Co nanoparticle embedded in porous nitrogen-doped CNFs, displaying a well-defined 3D network associated with an encapsulated and porous structure.^[152] The unique encapsulated structure could efficiently avoid the direct contact of metal nanoparticles with harsh environment, protecting the metal nanoparticles from corrosion and aggregation during the catalytic process. The porous structure could provide more active sites for the catalytic process and facilitate fast and versatile transport pathways for the electrolyte diffusion.

Benefiting from these, the material can serve as active electrocatalysts for both the OER and HER with an outstanding performance and excellent stability.

4.4. CO_2 Conversion

Carbon dioxide (CO_2) is the primary greenhouse gas, which has a significant effect on human's climate and environment. Owing to the unsustainable utilization of fossil fuels, the atmospheric concentration of CO_2 has rapidly increased, leading to global warming, drastic environmental problems, etc. Therefore, CO_2 conversion has been proposed as a potential way to maintain the balance of the carbon cycle and develop a sustainable society. Among the various technologies of catalytic conversion, naturally abundant and chemically stable TMs and their oxides have been explored as the potential catalysts,^[153–155] but the low efficiency and rapid loss of activity still remains due to the high overpotential. The chainmail catalyst accompanied with the high stability of TMs and the rather interesting behavior different from the naked TM nanoparticles, has been inducted into the CO_2 catalytic conversion recently.

Zhang et al. have constructed a nanostructure of Fe nanoparticle enclosed by ultrathin (1–3 layers) carbon layers ($\text{Fe}@C$) via using an Fe-containing metal-organic framework (MOF) (MIL-101) as both self-sacrificing template and precursor. Compared with naked Fe nanoparticles, the carbon layer-coated catalysts exhibited improved catalytic performance in the solar-driven CO_2 conversion by H_2 (Figure 7a), with a more stable CO_2 conversion speed and higher selectivity to CO through effectively coupling the light-harvesting and catalytic function in one material (Figure 7b). The mechanism analysis demonstrated that under photoirradiation, the local temperature of the nanoparticles increased dramatically, which can provide adequate energy to overcome the successive barrier and initiate the reaction process (Figure 7c). Simultaneously, the UV-light-induced Fe local surface-plasmon resonances activated the nonpolar molecules CO_2 , which produced enhancement of the CO_2 conversion in catalytic processes. DFT calculation results revealed that when few layers of graphene shell covered on Fe nanoparticles, the electron transfer from encapsulated Fe to graphene will happen (1.25 electrons by quantitative Bader charge analysis calculation), which decreased the work function of graphene surface (0.38 eV) (Figure 7d). It can dramatically promote desorption of produced CO from the catalyst surface while CO on the pure Fe surface is overbonded. Hence, through the electronic modulation of graphene by encapsulated Fe, the reaction selectivity to CO can be increased.^[156]

4.5. Dye-Sensitized Solar Cells

Solar energy and photovoltaic devices have attracted enormous interests due to energy depletion and environmental pollution brought by the over consumption of fossil fuels. Dye-sensitized solar cells (DSSCs), with low-cost fabrication, environmental friendliness, and relatively high power conversion efficiency, become a promising light-electricity device to address the challenge of achieving clean energy. Among the components

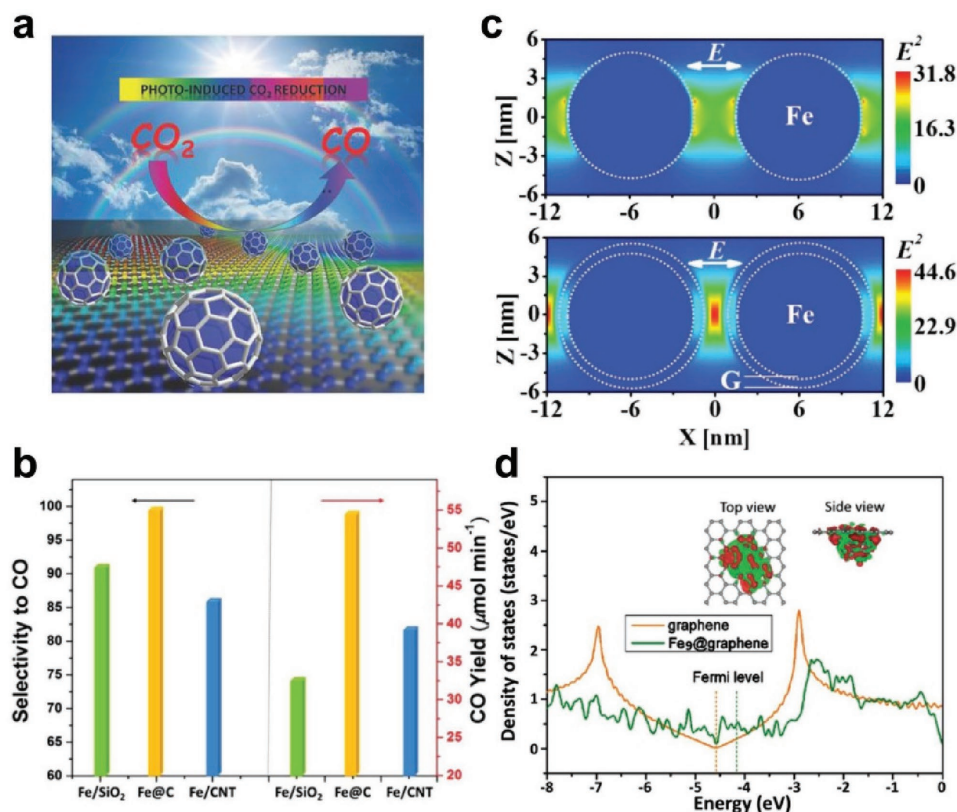


Figure 7. a) A schematic representation of the solar-driven reduction of CO₂ into CO process on the surface of Fe@C. b) Photoinduced thermocatalytic CO₂ conversion performance for Fe@C, Fe/SiO₂, and Fe/CNT catalysts in fixed bed reactor. c) Spatial distribution of the SPR-induced enhancement of electric field intensity at the SPR peak wavelength (350 nm), from FDTD simulation of 9 nm iron nanoparticles and 9 nm iron particles overcoated by multiple carbon layers. d) Projected density of states for the p_z orbitals of C atoms bonded with Fe atoms in the model of Fe₉@graphene in comparison with that of corresponding C atoms in pristine graphene model. a–d) Reproduced with permission.^[156] Copyright 2016, Wiley-VCH.

of DSSCs, the CE plays a vital role in improving the photovoltaic efficiency. The precious Pt is currently the most useful CE catalyst, but its limited resource and high-cost hindered the large-scale fabrication of DSSCs. Several catalytic materials like nonprecious-metal oxides or metal alloys have been proposed as potential alternatives to Pt catalyst, but there still remains a question for the electrochemical stability of the nonprecious-metal catalysts in electrolytes, due to the potential corrosion of metal CE in electrolytes by the formation of halides. In consideration of the stability when exploring high-performance nonprecious-metal catalysts in the CE of DSSCs, the chainmail catalyst can be a good choice.^[157–159]

Recently, Zheng et al. adopted the strategy to obtain an excellent CE electrocatalyst in the I⁻/I₃⁻ redox reaction of DSSCs (Figure 8a), through direct pyrolysis of organometallic precursors to prepare the podlike N-doped carbon nanotubes encapsulating FeNi alloy NPs (Pod(N)-FeNi) (Figure 8b). The Pod(N)-FeNi catalyst displayed significantly lower peak separation between the anodic and cathodic peaks (E_{pp}) of ≈60 mV (Figure 8c), lower charge transfer resistance (R_{ct}) of 0.54 Ω cm² at the interface of the CE/electrolyte (Figure 8d), higher exchange current density than the sputtered Pt counterpart (140 mA, 0.88 Ω cm²). Ultimately, the DSSC devices consisting of the Pod(N)-FeNi CE displayed a power conversion efficiency (PCE) of 8.82% (Figure 8e), superior to that of

the control device using sputtered Pt as the CE (PCE = 8.01%). Through the control experiments, it demonstrated that the existence of metal nanoparticles in the graphene shell can promote the electron transfer from the metal to the carbon shells. It will synergistically with nitrogen doping to change the electronic structure and reduce the surface work function of the carbon shells, consequently enhancing the catalytic activity of the carbon shells. More importantly, due to the FeNi alloy NPs were encapsulated by the graphene shells, they were protected from leaching and corrosion caused by the electrolyte, leading to a high stability during the sequential cyclic voltammetry (CV) scanning for 150 cycles with nearly no change of the current densities and the E_{pp} for Pod(N)-FeNi but noticeable decay in Pt CE.^[160]

Thereafter, the chainmail catalyst with encapsulated FeNi alloy has been constantly employed as the CE material of DSSCs through different prepared methods. For example, Zhu et al. used a simple and large-production pyrolysis approach to synthesize the onion-like nitrogen-doped carbon shell encapsulating FeNi₃ alloy (ONC@FeNi₃), which was exploited as catalyst for the triiodide reduction reaction in CE. The significantly lower peak-to-peak separation, lower charge-transfer resistance at the interface of the CE/electrolyte, and the higher exchange current density were found within the ONC@FeNi₃ catalyst. As a result, the DSSCs based on ONC@FeNi₃ achieved

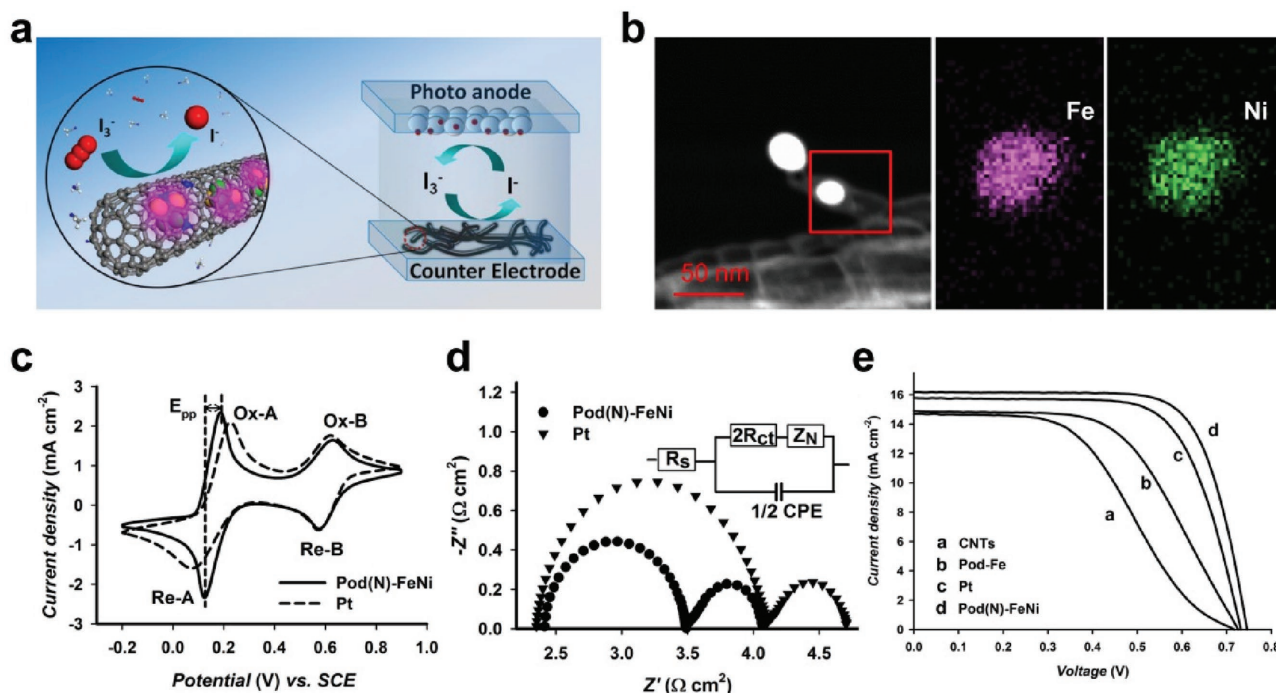


Figure 8. a) A schematic representation of the reduction of I_3^- to I^- process on the surface of Pod(N)-FeNi in the CE of DSSCs. b) Elemental mapping of the materials (the area in the box) reveal the homogeneous distribution of Fe and Ni elements in the metal nanoparticles. c) Cyclic voltammograms of the Pod(N)-FeNi and the sputtered Pt CEs. d) Electrochemical impedance spectra of symmetrical cells for Pod(N)-FeNi and the sputtered Pt CEs. e) Photocurrent density versus voltage (J - V) curves of the DSSCs using CNTs, Pod-Fe, Pt, and Pod(N)-FeNi as CEs. a-e) Reproduced with permission.^[160] Copyright 2014, Wiley-VCH.

outstanding power conversion efficiency (PCE) of 8.87%, which exceeded the 8.28% of Pt-based DSSCs. Furthermore, TEM investigation revealed that the N-doped graphitic carbon onions exhibit the high structural stability in iodine-containing medium even subject to hundreds of CV scanning.^[161] Similarly, Wu et al. also adopted a high-temperature thermal pyrolysis strategy to gain the NiFe alloy nanoparticle encapsulated in mesoporous nitrogen-doped carbon sphere (NiFe@MNCS).^[162] The DSSCs employing NiFe@MNCS CE could reach a PCE of 7.6%, very close to the DSSCs achieved by employing the Pt CE (7.8%), primarily owing to the presence of NiFe alloy nanoparticles that acted as a catalytic center for boosting the charge transfer process. With the protective carbon shell, the dissolution of NiFe alloy in corrosive iodide/iodine redox electrolyte could be suppressed, leading to an improved long-term stability of NiFe@MNCS CE. In addition, the electrospinning technique was employed by Saranya et al. to prepare bimetallic (Fe-Ni) nanoparticle embedded carbon nanofibers, which showed a superior electrocatalytic activity confirmed from the results of CV, electrochemical impedance spectroscopy and Tafel polarization studies.^[163]

Besides the FeNi alloy, other TM-based materials have been encapsulated as the CE catalyst. Xing et al. used a simple method to achieve different TM (Co and Ni) nanoparticles encapsulated in N-doped graphene shells that were applied into the CE of DSSCs. The experimental results indicate that both catalysts display high catalytic activity in the CE reduction reaction (I_3^- to I^-), and exhibit as the sequence of Ni > Co > Pt CE, considering the peak separation between the anodic and

cathodic peaks (E_{pp}), charge transfer resistance (R_{ct}), and Tafel curves. Furthermore, the corresponding photovoltaic devices made of the Co and Ni-based catalysts displayed efficiencies of 7.75% and 8.39%, respectively, which are comparable to or superior to that of the control sputtered Pt-based device with a PCE of 7.67%. The current densities and the E_{pp} experienced negligible change subject to CV measurements for 150 cycles, indicative of the superior stability of the Co and Ni-based catalysts in comparison with Pt CEs.^[57] Likewise, Wu et al. also developed a prepared method by thermal pyrolysis of Ni-organic framework under nitrogen environment followed with acid treatment to gain the Ni nanoparticles embedded in bimodal mesoporous carbon (BMCNi), which reached a cell efficiency of 8.6% when employing as CE catalyst outperforming the Pt CE (8.4%). The Ni nanoparticles embedded in BMC matrix offer electrical conductivity and extra active sites for expediting the I_3^-/I^- redox couple. The BMC with small and large mesopores not only provides numerous active sites for electrocatalytic reaction, but also accommodates large amounts of electrolyte for facilitating the transport of ions. In addition, the BMC matrix can protect the Ni nanoparticles from corrosion in the corrosive iodine-based electrolyte.^[164]

4.6. Metal-Air Batteries

Developing renewable energy generation and storage systems are drawing extensive attention because of the increasing global energy crisis and environmental issues caused by the heavy

reliance on fossil fuels. Rechargeable metal–air batteries (e.g., Zn–air and Li–air) with high theoretical energy densities have become promising technologies for future electronic vehicles and other advanced electronic devices. One of the pivotal tasks is to develop highly active and durable bifunctional electrocatalysts which can efficiently catalyze both the ORR and the OER in the discharge and charge processes, respectively. Although precious metals such as Pt, Ru, and Ir have been demonstrated to possess high activity in ORR or OER, however, these electrocatalysts are expensive and exhibit poor bifunctionality. In addition, precious-metal-based and nonprecious-metal electrocatalysts both also suffer from insufficient durability during the working conditions of metal–air batteries owing to the high overpotential and strong oxidative atmosphere. The unique chainmail catalysts have been found to be efficient electrocatalysts for both ORR and OER, and the graphene shell can enhance the durability of TMs against the corrosion of oxygen molecules during the discharge and charge processes. Therefore, recently the chainmail catalyst has been tried as the bifunctional oxygen electrode catalysts in the fields of metal–air batteries, especially the Zn–air and Li–air batteries.

4.6.1. Zn–Air Batteries

The Zn–air battery is a relatively mature technology compared to the Li–air battery, and its theoretical energy density can reach a value of 1086 W h kg⁻¹, which is approximately five times higher than that of current Li-ion batteries.^[165,166] Meanwhile, the Zn–air battery is environmentally benign, safe, and affordable.

Ding et al. employed a facile approach to prepare heteroatom-doped mesoporous carbons embedded with Fe₃C nanoparticles from a novel and low-cost Fe–histidine complex. The histidine with a high content of heteroatoms and high solubility in aqueous solutions, is a cheap and essential amino acid which can be found in various biological systems. The obtained catalysts exhibit excellent catalytic activity and stability for both ORR and OER, and subsequently high performance for rechargeable Zn–air batteries. The two-electrode Zn–air battery can exhibit an open-circuit voltage of 1.54 V, an energy density of 960 W h kg⁻¹, and a peak power density of 212 mW cm⁻². However, the battery discharge and charge performance deteriorated significantly at 20 mA cm⁻² under a long-term cycling test. Therefore, a three-electrode configuration was adopted to improve the cycling performance, which could prevent the bifunctional catalyst from coming into contact with the oxidative or reductive potential during discharge or charge process. Notably, in a three-electrode configuration, the rechargeable Zn–air battery exhibited excellent durability for operating at high current densities (20 and 50 mA cm⁻²) without obvious voltage loss.^[167] In addition, Zeng et al. also gain the metallic Co nanoparticles encapsulated in multilayered graphene shells prepared by the high-temperature decomposition of Co containing Prussian blue colloids, which can be used as the high-performance air catalyst of a Zn–air battery. The formed Zn–air battery has an open circuit voltage of ≈1.4 V, large current densities of 55 and 255 mA cm⁻² at a voltage of 1.2 and 1.0 V, and a maximum power density of close to 350 mW cm⁻². This Zn–air

battery is also very durable, when galvanostatically discharged at a current density of 10 mA cm⁻² for 14 h and 50 mA cm⁻² for 4.5 h, little activity decay is observed. The slight voltage loss is in fact associated with the degradation of Zn anode.^[168]

In view of the catalytic performance being strongly dependent on the structural and electronic properties of one catalytic material, the modulation and optimization within the chainmail catalyst matrix is of great importance. So aiming at the Zn–air batteries (Figure 9a), Zhu et al. designed a unique two-stage encapsulation technique with the aid of a MOF to acquire carbon-encapsulating Ni, Fe, or NiFe₂ alloy nanocrystals (denoted as Ni@NC_x, Fe@NC_x, NiFe@NC_x, respectively) (Figure 9b). They all possessed ultrasmall core size (7.8, 10.8, and 9.2 nm for NiFe@NC_x, Ni@NC_x, Fe@NC_x, respectively), high metal-loading (≈25 wt%), and high dispersion. The best NiFe@NC_x catalyst exhibits high stability and activity with an onset potential of 1.03 V for ORR and an overpotential for onset potential of only 0.23 V for OER (Figure 9c), superior to those of commercial Pt/C and IrO₂ catalysts. Rechargeable Zn–air batteries using NiFe@NC_x catalyst exhibited a small charge–discharge overpotential of 0.78 V at 50 mA cm⁻² (Figure 9d), high reversibility with a round-trip efficiency of 76.7% at 10 mA cm⁻², and high stability with only 0.29 V increase in the voltage gap after 205 cycles (Figure 9e). The superb electrocatalytic performance originates from the modulation of the electronic structure of outer carbon layers by electron penetration from the NiFe alloy. Reducing the size of encapsulated nanoalloy can significantly increase the active site density and the electron density in the graphene shells, which further enhance the ORR and OER activities.^[169]

Similarly, Wang et al. successfully synthesized high-density Fe nanoparticles encapsulated into nitrogen-doped carbon nanoshells (Fe@N–C) by solid-phase precursor's pyrolysis of dicyandiamide and ammonium ferric citrate followed with acid-leaching. The optimized high-density catalyst showed excellent bifunctionality for ORR and OER in alkaline medium compared to state-of-the-art commercial Pt/C and IrO₂. Furthermore, the Zn–air battery constructed with the Fe@N–C catalyst exhibits the maximum peak power density of 220 mW cm⁻² at 0.72 V, which is higher than those of Pt/C (192 mW cm⁻² at 0.63 V) and IrO₂ (141 mW cm⁻² at 0.50 V). The initial charge and discharge potential of Fe@N–C catalyst is ≈1.95 and ≈1.25 V. After 10 cycles, the values change to ≈1.97 and ≈1.11 V, and these values are stable until 100 cycles, showing excellent cycling durability of the catalyst in rechargeable Zn–air batteries.^[170]

4.6.2. Li–Air Batteries

The Li–air battery possesses exceptionally high theoretical specific energy density (up to 2000–3000 W h kg⁻¹), rivaling that of any other existing rechargeable batteries and can even be comparable to gasoline.^[171–173] In consideration of this aspect, rechargeable Li–air batteries are being regarded as a promising candidate for next-generation energy-storage system. Until now, a critical scientific challenge facing Li–air batteries is the high charge overpotential due to the sluggish OER on the oxygen electrode, which results in low energy efficiency and poor cyclability.^[174–176]

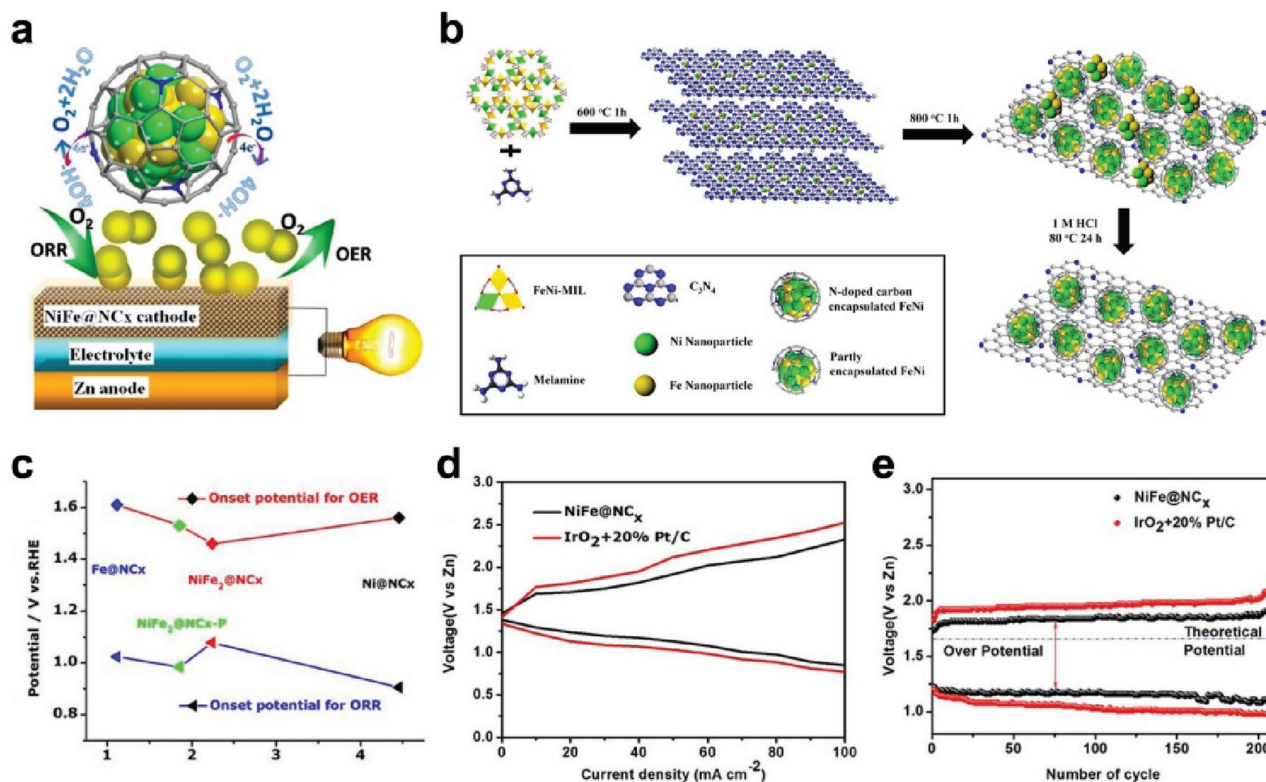


Figure 9. a) A schematic representation of the ORR and OER processes on the surface of NiFe@NC_x in the rechargeable Zn–air batteries. b) Schematic illustration of the synthetic strategy of the TMs@NC_x composite. c) The pyridinic N content versus onset potential for ORR and OER of TMs@NC_x catalysts. d) Charge and discharge polarization curves for the Zn–air batteries. e) Cycle stability of the rechargeable Zn–air battery. The galvanostatic discharge–charge cycling curves were performed at 10 mA cm^{−2} with a duration of 600 s per cycle. Reproduced with permission.^[169] Copyright 2016, American Chemical Society.

Tu et al. recently prepared a highly efficient oxygen electrode catalyst for Li–air batteries (Figure 10a), i.e., N-doped single layer graphene shell encapsulating nonprecious-metal Co (Co@NC) (Figure 10b). The experiments showed that the graphene shells can protect the metals from being oxidized in O₂ atmosphere. Moreover, the electronic structure of graphene shell can be modulated by N dopants and encapsulated metal nanoparticles to enhance both ORR and OER activity, leading to the lower discharge/charge overpotential in Li–air batteries. In particular, Co@NC electrode delivers high catalytic activity with discharge and charge overpotentials of 0.14 and 0.58 V, which was remarkably lower compared with the corresponding N-free graphene encapsulating metal, metal oxide, and metal-free carbon materials (Figure 10c). Moreover, the Co@NC based electrode showed a better cycling performance than graphene and CNTs based electrodes (Figure 10d). DFT calculations revealed that the electrons from encapsulated transition metals can enhance the charge density of the carbon layers. Moreover, with the N dopants, this enhancement of charge density will become much more apparent, which can synergistically modulate the electronic properties of the graphene surface. Thus it changed the thermodynamic free energies of the intermediates of each reaction steps and affected the potential difference between these steps (Figure 10e), and ultimately resulting in a dramatic decrease in the voltage gap. It provides the possibility for the rational design of nonprecious-metal catalysts toward Li–air batteries.^[177]

Apart from the design of chainmail catalyst within nonprecious-metal catalysts, other studies have also adopted this distinct strategy for the adjustment of precious-metal based catalysts to overcome their instabilities and reduce the overpotentials. For example, Guo et al. developed a novel oxygen cathode by encapsulating RuO₂ nanoparticles into nanoporous N-doped graphene to stabilize the RuO₂ nanoparticles.^[178] The obtained catalyst owns high catalytic activity and ultrahigh stability, showing highly reversible cathodic reactions for up to 100 time discharge/charge cycles at the cutoff capacity of 2000 mA h g_{total}^{−1} and low average charge potential of 3.7 V. Although the RuO₂ nanoparticles are encapsulated by graphene which prevents the direct contact of the catalysts with the electrolyte and Li₂O₂, the catalytic nanoparticles still show high catalytic activities toward cathodic reactions, similar to the recent observations of Tu et al. Meanwhile, the RuO₂ nanoparticles are stabilized by graphene surrounding for long cycling lifetime.

Additionally, Huang et al. also encapsulated a series of precious-metal nanoparticles (Pd, Pt, Ru, and Au) inside graphitic carbon shells, which exhibit a dramatic reduction of charge overpotentials compared to their counterparts with nanoparticles directly supported on carbon surface. Especially, the charge overpotential can be as low as 0.3 V and good stability during discharge–charge cycling can be achieved when Pd-based catalyst is used on the cathode. DFT calculations reveal that encapsulation of “guest” precious-metal

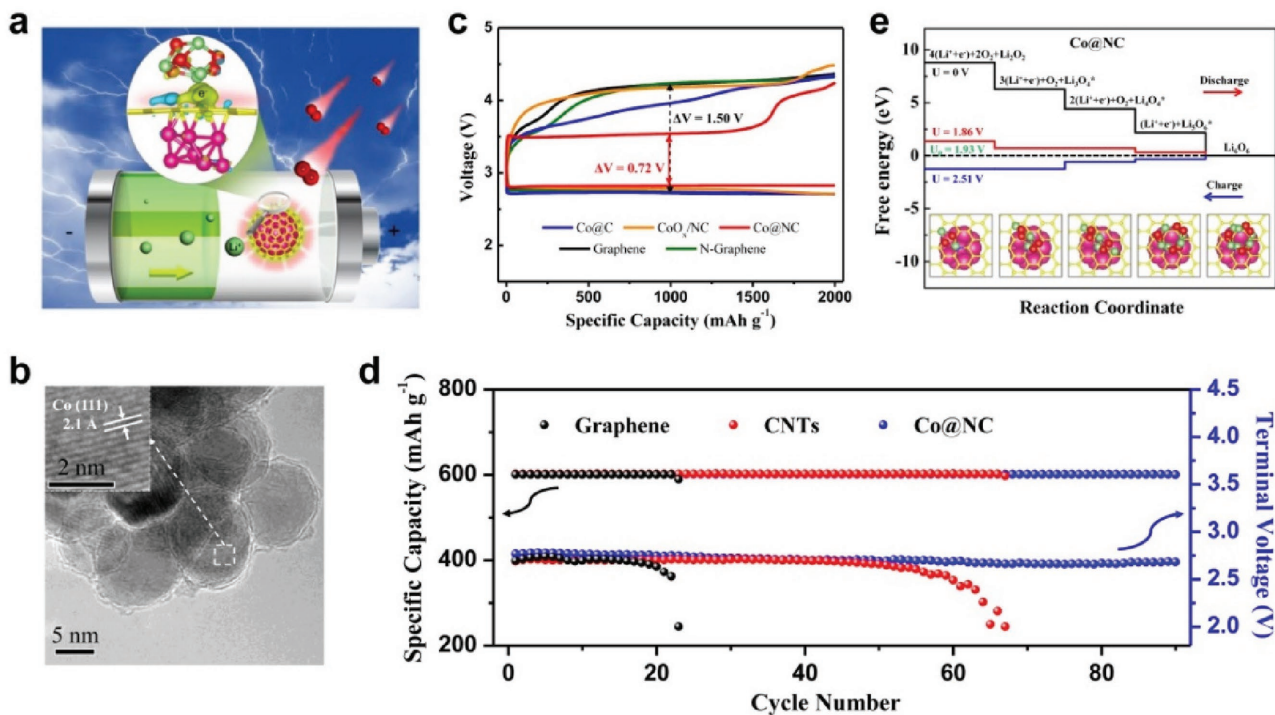


Figure 10. a) A schematic representation of the charge–discharge process on the surface of Co@NC in the Li–air batteries. b) HRTEM image of Co@NC with the inset showing the (111) crystal plane of the Co particle. c) Discharge/charge profiles of the Li–air batteries with different cathodes at a current density of 200 mA g^{-1} with the fixed capacity of 2000 mA h g^{-1} . d) Cycling stability and the terminal discharge voltage as a function of cycle number for the graphene-, CNTs-, and Co@NC-based cathodes for Li–air batteries. e) Calculated free energy diagram for the oxygen electrode reactions along M2 on the surface of N-doped graphene encapsulating Co nanoparticles (Co@NC). Reproduced with permission.^[177] Copyright 2016, Elsevier.

nanoparticles in “host” carbon shell is able to strengthen the electron density on carbon surfaces, and to avoid the regional enrichment of electron density caused by the direct exposure of nanoparticles on carbon surface. These unique properties ensure the uniform coverage of Li_2O_2 nanocrystals on carbon surfaces instead of localized distribution of Li_2O_2 aggregation, thus providing efficient charge transfer for the decomposition of Li_2O_2 .^[179]

4.7. Catalytic Hydrogenation

In the industrial and pharmaceutical fields, catalytic hydrogenation process is an important kind of reaction for the production of fine and bulk chemicals. Precious metals such as Ru, Pd, Ir, Pt, and Au have been proved to be active components for catalytic hydrogenation process. However, considering the high price and limited availability of precious metals, it is necessary to develop nonprecious-metal catalysts. TM nanoparticles have attracted intense scientific interest in the past few decades because of their excellent physicochemical properties and promising applications in a variety of fields. Unfortunately, naked TM nanoparticles are easy to agglomerate during usage because of their high surface energy and high reactivity, which is a major limitation to their practical applications. Therefore, fabricating chainmail catalyst with the TMs to promote the catalytic activity on the outermost shell surface and the protective shell to prevent the harm to the inner TMs, is a feasible strategy

to increase the stability of nonprecious-metal catalyst under this reaction condition.

Hu et al. have lately designed a facile strategy to fabricate FeCo nanocrystals inside N-doped graphene shells, involving one-step thermal decomposition of Prussian blue analogue $\text{Fe}_3[\text{Co}(\text{CN})_6]_2$ spheres. The as-prepared catalyst was employed to catalyze the hydrogenation of 4-nitrophenol to 4-aminophenol by NaBH_4 at room temperature. The estimated completion time of the catalyst was about 350 s, and the kinetic constant k_{app} was $8.28 \times 10^{-3} \text{ s}^{-1}$ (0.4968 min^{-1}), which is comparable to that of some precious-metal catalysts for catalytic hydrogenation of 4-nitrophenol. Furthermore, the conversion of 4-nitrophenol can be achieved above 95% even after running for ten cycles, indicating a stable catalytic performance. The excellent catalytic activity may originate from that the synergistic effect of FeCo nanocrystals and nitrogen dopants promoted the hydrogenation reaction, and the relatively small size of FeCo nanocrystals greatly improved the utilization efficiency of the metal nanoparticles.^[180]

The hydrogenation of 4-nitrophenol process has also been investigated by Li et al.^[181] In their study, hierarchically porous N-doped carbon frameworks embedded with Co nanoparticles (Co@NC) were prepared by a MOF-engaged strategy using a well-defined rhombic dodecahedral Co-based zeolitic imidazolate framework-67 (ZIF-67-Co) as an effective precursor and template (Figure 11a). Numerous small particles with diameters of about 8 nm are uniformly distributed in the carbon frameworks and several nanopores are distributed homogeneously

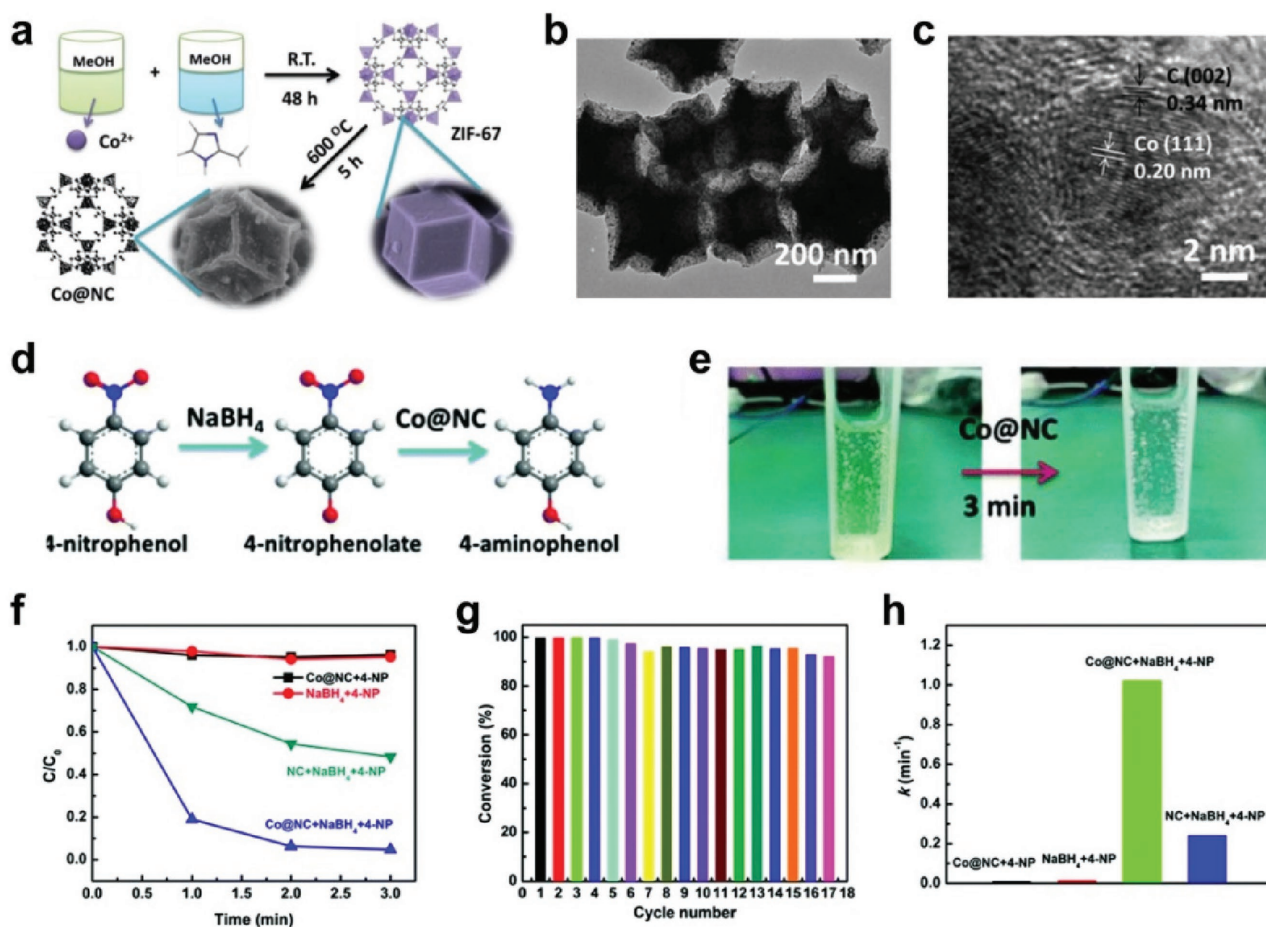


Figure 11. a) Schematic illustration of the synthesis of Co@NC derived from ZIF-67-Co. b) TEM image of the Co@NC. c) HRTEM image of the Co@NC with the Co nanoparticle completely covered by carbon layers. d) Reduction reaction for the conversion of 4-nitrophenol to 4-aminophenol catalyzed by Co@NC in the presence of NaBH₄. e) Pictures of the reduction of 4-nitrophenol by NaBH₄ before and after being catalyzed by Co@NC. f) Catalytic efficiency in different systems for 4-nitrophenol reduction as a function of time. g) Reusability test of the Co@NC for the catalytic reduction of 4-nitrophenol. h) Kinetic constants of different systems for 4-nitrophenol reduction. a–h) Reproduced with permission.^[181] Copyright 2016, Royal Society of Chemistry.

throughout the whole rhombic dodecahedron (Figure 11b,c), allowing efficient diffusion, transportation, and transfer of reactants to the catalytically active sites. The resulting Co@NC exhibited remarkable catalytic activity and excellent durability for the catalytic hydrogenation of 4-nitrophenol to 4-aminophenol by NaBH₄ in an aqueous solution (Figure 11d). It could reach nearly 100% conversion within 3 min (Figure 11e,f), even when the amount of the catalyst used was as low as 0.02 mg. Moreover, after 17 successive cycles of reactions, it still retained large conversion efficiencies over 95% (Figure 11g). The apparent rate constant for the catalytic reaction of 4-aminophenol hydrogenation was estimated to be 1.024 min⁻¹ (Figure 11h), which was superior to those of the previously reported TM nanoparticles and even compared favorably with that of the most active precious-metal nanoparticles.

Beyond the reaction systems of catalytic hydrogenation of 4-nitrophenol to 4-aminophenol, the unique chainmail catalyst can be used for the transfer hydrogenation of nitriles to imines. Long et al. report a facile and repeatable route to synthesize TM based nanocatalysts by first developing a series of

new and novel N-donor multimetallic M–M′-MOFs [(M–M′(1,4-bdc)₂(dabco))·4DMF·1/2H₂O, M/M′ = Co, Ni, Cu) through a facile mixed-metal approach and then directly pyrolyzing these heteronuclear MOFs under inert gas. In the pyrolysis process, the TM ions (two of Co, Ni, and Cu) of M–M′-MOFs could be transformed into transition alloy nanoparticles while the surrounding N-containing ligands were polymerized to N-doped graphitic carbon, resulting in highly dispersed M/M′ alloy nanoparticles embedded in the N-doped carbon matrix. The alloy nanoparticles were highly dispersed and embedded in the highly ordered N-doped graphene layers with an average size of ≈20 nm (denoted as M–M′@C–N). The TM elements were completely alloyed and the N-doped carbon was homogeneously distributed on every nanoparticle. When being used in the transfer hydrogenation of nitriles in the absence of basic additives, the optimal Co–Ni(3:1)@C–N showed the best catalytic performance with 100% conversion of benzonitrile and over 98% yield for the desired product, which was almost 5 times more active than its monometallic counterparts. It was found that nitriles substituted with electron-donating groups,

such as methyl and methoxyl, underwent the transfer hydrogenation reaction smoothly to afford the corresponding imines in excellent yields, while nitriles substituted with electron-withdrawing groups, especially halogenated nitriles, are more challenging to be hydrogenated due to the competition with dehalogenation.^[182]

4.8. Syngas Conversion

The syngas (H_2/CO), derived from coal, natural gas or biomass etc., is an important feedstock for the production of useful hydrocarbons, fuels, and other chemicals in the industrial process. During the syngas conversion process, metal catalysts especially the nonprecious-metal 3d TM nanocatalysts (such as Fe, Co, and Ni) become the first choice considering the economic cost and earthly storage.^[183] However, the 3d TM catalysts face significant problems such as the coking and sintering under high temperature, leading to the deactivation of the catalyst. One of the solved methods is to coating the metal nanoparticles with a protection layer to stabilize them, but still maintain their necessary electronic conductivity and chemical activity as catalysts. It is because the protection layer with electronically poorly conduction such as organic molecules, polymers, or oxides, etc. may block effective charge transfer between the catalysts and the reagents, and thus reduce the electrical conductivities and work functions of metal nanoparticles.^[184–186] The graphene with extremely high electron mobility up to $15\,000\text{ cm}^2\text{ V}^{-1}\text{ s}$ at room temperature is a good option to protect the inner metal particles from harsh reaction conditions,^[20,187] while the penetration electron of the TMs promote the catalytic reaction on the graphene surface. In consideration of these, the chainmail catalyst has recently been applied into the field of syngas conversion.

Chen et al. demonstrated that Fe nanoparticles encapsulated in pod-like carbon nanotubes (Pod-Fe) can be used as an efficient catalyst to achieve the conversion of syngas into light olefins via the Fischer–Tropsch synthesis. It gave a higher selectivity of light olefins (45%) and high stability over 120 h reaction ($P = 0.5\text{ MPa}$, $T = 320\text{ }^\circ\text{C}$, $CO:H_2 = 1:2$, gas hourly space velocity = 3500 h^{-1}). A catalyst with exposed Fe particles on the outside of the Pod-Fe ($FeO_x/\text{Pod-Fe}$) catalyst showed a selectivity of light olefins of 42%, but had a significantly lower stability. In order to find the reason for the deactivation of $FeO_x/\text{Pod-Fe}$ at high temperature, TEM characterization was carried out. It showed that the Pod-Fe catalyst still kept the morphology of the pod-like structure even after reaction at $380\text{ }^\circ\text{C}$ for 10 h, and no obvious agglomerated Fe and carbon filaments were observed. In contrast, the tube morphology of the $FeO_x/\text{Pod-Fe}$ was hardly observed after 10 h reaction at $340\text{ }^\circ\text{C}$, the Fe particles were agglomerated and the tubular structure was covered by carbon filaments and flakes. The authors interpreted that there is a strong interaction between encapsulated nonprecious metals and the carbon shell, which lead to electron transfer from Fe to the carbon shell and reduced the local work function of the carbon surface where the Fe particles were located. Then the penetrated electron from the Fe to the outside carbon surface probably promoted the adsorption of CO and H_2 , and their subsequent activation since the Fe was encapsulated

inside the compartment of the pod-like carbon nanotubes and cannot directly contact the reaction molecules. Meanwhile, the stable carbon shells effectively protected the inner Fe from agglomeration. Hence, the Pod-Fe catalyst ultimately showed good selectivity toward light olefins and excellent antisintering performance.^[188]

Focusing on the Fischer–Tropsch synthesis, Wang et al. also report a one-step simple route to in situ prepare graphene-encapsulating Fe nanoparticles ($Fe@G$) with the Fe nanoparticles of 5–15 nm diameter and graphene of two to five layers via an arc-discharge method. As a catalyst for syngas conversion, it exhibits excellent catalytic performance with a stable CO conversion ($\approx 75\%$) and a high yield on light olefins ($C_2\text{--}C_4$, $746\text{ mg g}_{\text{cat}}^{-1}\text{ h}^{-1}$) and C_{5+} hydrocarbon ($706\text{ mg g}_{\text{cat}}^{-1}\text{ h}^{-1}$) at 553 K , which is more than three times that of bare Fe nanoparticles. The graphene shell was proposed to be responsible for the olefins favorable and chain growing enhancing for heavy hydrocarbon products. Furthermore, the $Fe@G$ shows no apparent changes on nanoparticles' size and morphology, and the graphene shell still survives after the catalytic reaction.^[189]

Apart from encapsulating Fe nanoparticle to catalyze syngas conversion via the Fischer–Tropsch synthesis, the Ni nanoparticles can be introduced into the graphene shell to achieve the conversion of syngas from the gasification of coal or biomass into synthetic natural gas via the methanation reaction. Wang et al. adopted the arc-discharge method to in situ prepare graphene-encapsulating Ni nanoparticles ($Ni@G$). The Ni nanoparticles with diameter 5–15 nm are encapsulated by 2–4 layers of graphene. Moreover, when NH_3 is introduced into the reaction atmosphere during the arc discharge process, Ni nanoparticles encapsulated in N-doped graphene ($Ni@G\text{--}N$) can be obtained. The $Ni@G$ catalyst exhibit excellent catalytic performance for the methanation reaction, and the catalytic performance is further improved when the graphene shell is doped with nitrogen ($Ni@G\text{--}N$). Particularly, it can deliver highly stable CO conversion ($\approx 99\%$ at $450\text{ }^\circ\text{C}$) and a high yield of methane ($\approx 91\%$ at $450\text{ }^\circ\text{C}$), which is better than that of bare Ni nanoparticles. Furthermore, the unique confinement effect of the graphene shell leads to good resistance to sintering and carbon deposition in this high-temperature reaction. The electron transfer between Ni nanoparticles and the graphene layer facilitate the adsorption and reaction behavior of H_2 and CO on the catalyst surface, and the N-doping in the graphene shell will create higher carrier density for efficient electron transfer, which may benefit a further enhanced catalytic performance of $Ni@G$. In addition, further modification of the graphene shell by the hydrogen activation process to remove the absorbed groups, heal the defects of graphene shell and enhance the crystalline quality of graphene sheath, can also improve the catalytic performance of the catalyst.^[190]

5. Perspective

The chainmail catalyst, with the concept of electron penetration through 2D crystal layer to strengthen the catalytic performance on the 2D material surface, has exhibited considerable advantages toward various reaction systems (Table 1), especially the catalytic processes conducted under harsh conditions (e.g.,

strong acidity or alkalinity, high temperature, and high overpotential). However, in view of both the fundamental research and industrial application, this still remains some challenges.

The precise control and modulation of structural and electronic properties within the 2D crystal encapsulating TM catalyst is still a difficult issue. For example, the optional combination between the TMs and 2D crystal shells is far from sufficient at present. The graphene now occupied the dominant position among the species of shells for encapsulation due to the well-developed strategy for the preparation of graphene, while using other 2D materials as the shells still needs quantities of trial and error. In addition, considering that the layer thickness of graphene will significantly affect the electron penetration accompanied with different catalytic performance, the accurate layer number control of the graphene shell still needs to be reinforced, despite the graphene layer covering the TMs can be reduced to single layer. Also, the stability of the graphene shell should be taken into account, for that single graphene layer may be easily damaged and two to three layers could be a compromised choice for the graphene shell. Introducing heteroatoms into the graphene matrix has been proved to be effective to modulate the electronic properties of surface carbon atom synergistically with TM nanoparticles. However, the most dopants are the N atoms and few are the B, P atoms. It should be also interesting to dope more heteroatoms such as S, Se, Cl, etc. into the graphene shell and thereby to study their effect on the electronic and catalytic properties of graphene shells.

In addition, currently, the TMs mainly focus on only few 3d metals (e.g., Fe, Co, Ni, and Cu) and their compounds, so new methods are required to encapsulate other more sorts of TMs into 2D crystal shells to bring novel electronic and catalytic properties. At the same time, the particle size of the TMs is also hard to be tuned in a controllable and uniform range, which is of vital importance because the particle size will influence the utilization efficiency of the metal particle and subsequently the transfer efficiency of electrons from the TMs.

In spite of various prepared methods have been developed for the chainmail catalyst synthesis, usually one method can only synthesize one or few specified structures. There is still lack of a universal technique to achieve the structural polytrope toward the framework of 2D materials and TMs. Moreover, most of the prepared processes are not economical, such as many precursors are still expensive, the high-temperature treatment and the complicated procedure needs high energy consumption and additional maintenance of instruments. Therefore, more sustainable and facile routes are required for the production of the chainmail catalyst, e.g., biomass or crop wastes can be used as the low-cost and widely available precursors for the synthesis. Another significant issue is to realize the large-scale production to meet the needs of industrial application in catalysis, which now still remains a big challenge.

The catalytic mechanism study is important for the understanding of reaction process and improvement of catalytic performance, and also in reverse for the structural and electronic design and modulation of the chainmail catalyst. Although the electronic properties and catalytic nature on the 2D material surface with TMs underneath have been investigated in detail by both experiments and theoretical calculations, there is lack of effective characterization tools to in situ observe the electron

transfer process and the corresponding variation of structural and electronic properties during the catalytic reaction. In addition, the definite structure provides a well-defined model to bridge the theoretic study and realistic systems, but a big gap between them still remains. It is urgent to develop more effective in situ characterization techniques and theoretical calculation methods to understand the catalytic nature and process.

While the chainmail catalyst has exhibited considerable potential in catalysis from scientific prospect, there are a number of technological problems that waiting to be solved. One of the significant issues is to mold or assemble the chainmail catalyst into a real industrial catalyst, but they usually tend to aggregate or sinter under the conditions of high overpotential or high temperature due to their loose structures. One of the effective ways is to construct 3D skeleton with the catalyst anchored into stable supports, such as SiC, carbon fiber, metal porous foam, etc. In addition, the mechanical strength, mass transport, solvophilic feature, electric conductivity, etc. also should be taken into overall consideration toward a real industrial catalytic process.

Although there is still some challenges for the fundamental research and industrial applications of these chainmail catalysts, we believe that the insights of the chainmail catalysts will be increasingly enhanced, and there is a surely promising future for the industrial applications by developing appropriate preparation strategy, controlling their structural and electronic properties, and understanding the catalytic nature and process through combining in situ characterizations and theoretical calculations.

Acknowledgements

The authors gratefully acknowledge financial support from the Ministry of Science and Technology of China (No. 2016YFA0204100 and 2016YFA0200200), the National Natural Science Foundation of China (No. 21573220 and 21621063), the Key Research Program of Frontier Sciences of the Chinese Academy of Sciences (No. QYZDB-SSW-JSC020), and the strategic Priority Research Program of the Chinese Academy of Sciences (No. XDA09030100).

Conflict of Interest

The authors declare no conflict of interest.

Keywords

2D materials, chainmail for catalyst, electron penetration, graphene, nonprecious metals

Received: December 26, 2016

Revised: May 31, 2017

Published online: September 22, 2017

- [1] A. Balanta, C. Godard, C. Claver, *Chem. Soc. Rev.* **2011**, *40*, 4973.
- [2] X. F. Yang, A. Q. Wang, B. T. Qiao, J. Li, J. Y. Liu, T. Zhang, *Acc. Chem. Res.* **2013**, *46*, 1740.
- [3] B. H. Wu, Y. J. Kuang, X. H. Zhang, J. H. Chen, *Nano Today* **2011**, *6*, 75.

- [4] S. Koh, P. Strasser, *J. Am. Chem. Soc.* **2007**, *129*, 12624.
- [5] B. H. Wu, N. F. Zheng, *Nano Today* **2013**, *8*, 168.
- [6] N. Tian, Z. Y. Zhou, S. G. Sun, Y. Ding, Z. L. Wang, *Science* **2007**, *316*, 732.
- [7] S. Linic, P. Christopher, D. B. Ingram, *Nat. Mater.* **2011**, *10*, 911.
- [8] H. Tada, T. Kiyonaga, S. Naya, *Chem. Soc. Rev.* **2009**, *38*, 1849.
- [9] S. Linic, U. Aslam, C. Boerigter, M. Morabito, *Nat. Mater.* **2015**, *14*, 567.
- [10] Y. Y. Liang, Y. G. Li, H. L. Wang, J. G. Zhou, J. Wang, T. Regier, H. J. Dai, *Nat. Mater.* **2011**, *10*, 780.
- [11] X. W. Xie, Y. Li, Z. Q. Liu, M. Haruta, W. J. Shen, *Nature* **2009**, *458*, 746.
- [12] J. Wang, Y. Li, Y. Zhang, *Adv. Funct. Mater.* **2014**, *24*, 7073.
- [13] D. H. Deng, L. Yu, X. Q. Chen, G. X. Wang, L. Jin, X. L. Pan, J. Deng, G. Q. Sun, X. H. Bao, *Angew. Chem. Int. Ed.* **2013**, *52*, 371.
- [14] D. H. Deng, K. S. Novoselov, Q. Fu, N. F. Zheng, Z. Q. Tian, X. H. Bao, *Nat. Nanotechnol.* **2016**, *11*, 218.
- [15] F. Yang, D. H. Deng, X. L. Pan, Q. Fu, X. H. Bao, *Natl. Sci. Rev.* **2015**, *2*, 183.
- [16] X. Q. Chen, J. P. Xiao, J. Wang, D. H. Deng, Y. F. Hu, J. G. Zhou, L. Yu, T. Heine, X. L. Pan, X. H. Bao, *Chem. Sci.* **2015**, *6*, 3262.
- [17] M. Merckx, D. A. Kopp, M. H. Sazinsky, J. L. Blazyk, J. Muller, S. J. Lippard, *Angew. Chem. Int. Ed.* **2001**, *40*, 2782.
- [18] G. I. Panov, A. K. Uriarte, M. A. Rodkin, V. I. Sobolev, *Catal. Today* **1998**, *41*, 365.
- [19] A. K. Geim, K. S. Novoselov, *Nat. Mater.* **2007**, *6*, 183.
- [20] S. S. Chen, L. Brown, M. Levendorf, W. W. Cai, S. Y. Ju, J. Edgeworth, X. S. Li, C. W. Magnuson, A. Velamakanni, R. D. Piner, J. Y. Kang, J. Park, R. S. Ruoff, *ACS Nano* **2011**, *5*, 1321.
- [21] K. S. Novoselov, D. Jiang, F. Schedin, T. J. Booth, V. V. Khotkevich, S. V. Morozov, A. K. Geim, *Proc. Natl. Acad. Sci. USA* **2005**, *102*, 10451.
- [22] D. H. Deng, X. L. Pan, H. Zhang, Q. A. Fu, D. L. Tan, X. H. Bao, *Adv. Mater.* **2010**, *22*, 2168.
- [23] D. H. Deng, L. Yu, X. L. Pan, S. Wang, X. Q. Chen, P. Hu, L. X. Sun, X. H. Bao, *Chem. Commun.* **2011**, *47*, 10016.
- [24] K. S. Novoselov, A. K. Geim, S. V. Morozov, D. Jiang, Y. Zhang, S. V. Dubonos, I. V. Grigorieva, A. A. Firsov, *Science* **2004**, *306*, 666.
- [25] C. O. Girit, J. C. Meyer, R. Erni, M. D. Rossell, C. Kisielowski, L. Yang, C. H. Park, M. F. Crommie, M. L. Cohen, S. G. Louie, A. Zettl, *Science* **2009**, *323*, 1705.
- [26] O. Cretu, A. V. Krasheninnikov, J. A. Rodriguez-Manzo, L. T. Sun, R. M. Nieminen, F. Banhart, *Phys. Rev. Lett.* **2010**, *105*, 196102.
- [27] H. T. Wang, Q. X. Wang, Y. C. Cheng, K. Li, Y. B. Yao, Q. Zhang, C. Z. Dong, P. Wang, U. Schwingenschlogl, W. Yang, X. X. Zhang, *Nano Lett.* **2012**, *12*, 141.
- [28] J. Zhao, Q. M. Deng, A. Bachmatiuk, G. Sandeep, A. Popov, J. Eckert, M. H. Rummeli, *Science* **2014**, *343*, 1228.
- [29] R. Bashyam, P. Zelenay, *Nature* **2006**, *443*, 63.
- [30] M. Lefevre, E. Proietti, F. Jaouen, J. P. Dodelet, *Science* **2009**, *324*, 71.
- [31] E. Proietti, F. Jaouen, M. Lefevre, N. Larouche, J. Tian, J. Herranz, J. P. Dodelet, *Nat. Commun.* **2011**, *2*, 416.
- [32] D. H. Deng, X. Q. Chen, L. Yu, X. Wu, Q. F. Liu, Y. Liu, H. X. Yang, H. F. Tian, Y. F. Hu, P. P. Du, R. Si, J. H. Wang, X. J. Cui, H. B. Li, J. P. Xiao, T. Xu, J. Deng, F. Yang, P. N. Duchesne, P. Zhang, J. G. Zhou, L. T. Sun, J. Q. Li, X. L. Pan, X. H. Bao, *Sci. Adv.* **2015**, *1*, e1500462.
- [33] X. J. Cui, J. P. Xiao, Y. H. Wu, P. P. Du, R. Si, H. X. Yang, H. F. Tian, J. Q. Li, W. H. Zhang, D. H. Deng, X. H. Bao, *Angew. Chem. Int. Ed.* **2016**, *55*, 6707.
- [34] X. Q. Chen, L. Yu, S. H. Wang, D. H. Deng, X. H. Bao, *Nano Energy* **2017**, *32*, 353.
- [35] A. H. Castro Neto, F. Guinea, N. M. R. Peres, K. S. Novoselov, A. K. Geim, *Rev. Mod. Phys.* **2009**, *81*, 109.
- [36] J. Greeley, J. K. Norskov, M. Mavrikakis, *Annu. Rev. Phys. Chem.* **2002**, *53*, 319.
- [37] D. H. Deng, X. L. Pan, L. A. Yu, Y. Cui, Y. P. Jiang, J. Qi, W. X. Li, Q. A. Fu, X. C. Ma, Q. K. Xue, G. Q. Sun, X. H. Bao, *Chem. Mater.* **2011**, *23*, 1188.
- [38] Y. Jiao, Y. Zheng, M. Jaroniec, S. Z. Qiao, *J. Am. Chem. Soc.* **2014**, *136*, 4394.
- [39] J. Lee, H. Kim, S. J. Kahng, G. Kim, Y. W. Son, J. Ihm, H. Kato, Z. W. Wang, T. Okazaki, H. Shinohara, Y. Kuk, *Nature* **2002**, *415*, 1005.
- [40] D. J. Hornbaker, S. J. Kahng, S. Misra, B. W. Smith, A. T. Johnson, E. J. Mele, D. E. Luzzi, A. Yazdani, *Science* **2002**, *295*, 828.
- [41] Y. Xie, J. M. Zhang, Y. P. Huo, *Eur. Phys. J. B* **2011**, *81*, 459.
- [42] C. K. Yang, J. Zhao, J. P. Lu, *Phys. Rev. Lett.* **2003**, *90*, 257203.
- [43] R. V. Jagadeesh, A. E. Surkus, H. Junge, M. M. Pohl, J. Radnik, J. Rabeah, H. M. Huan, V. Schunemann, A. Bruckner, M. Beller, *Science* **2013**, *342*, 1073.
- [44] G. Wu, K. L. More, C. M. Johnston, P. Zelenay, *Science* **2011**, *332*, 443.
- [45] J. Deng, L. Yu, D. H. Deng, X. Q. Chen, F. Yang, X. H. Bao, *J. Mater. Chem. A* **2013**, *1*, 14868.
- [46] J. Deng, P. J. Ren, D. H. Deng, X. H. Bao, *Angew. Chem. Int. Ed.* **2015**, *54*, 2100.
- [47] F. Guinea, *Phys. Rev. B* **2007**, *75*, 235433.
- [48] H. A. Chen, C. L. Hsin, Y. T. Huang, M. L. Tang, S. Dhuey, S. Cabrini, W. W. Wu, S. R. Leone, *J. Phys. Chem. C* **2013**, *117*, 22211.
- [49] X. J. Cui, P. J. Ren, D. H. Deng, J. Deng, X. H. Bao, *Energy Environ. Sci.* **2016**, *9*, 123.
- [50] L. S. Panchokarla, K. S. Subrahmanyam, S. K. Saha, A. Govindaraj, H. R. Krishnamurthy, U. V. Waghmare, C. N. R. Rao, *Adv. Mater.* **2009**, *21*, 4726.
- [51] Z. W. Liu, F. Peng, H. J. Wang, H. Yu, W. X. Zheng, J. A. Yang, *Angew. Chem. Int. Ed.* **2011**, *50*, 3257.
- [52] S. B. Yang, L. J. Zhi, K. Tang, X. L. Feng, J. Maier, K. Mullen, *Adv. Funct. Mater.* **2012**, *22*, 3634.
- [53] D. C. Wei, Y. Q. Liu, Y. Wang, H. L. Zhang, L. P. Huang, G. Yu, *Nano Lett.* **2009**, *9*, 1752.
- [54] J. Deng, P. J. Ren, D. H. Deng, L. Yu, F. Yang, X. H. Bao, *Energy Environ. Sci.* **2014**, *7*, 1919.
- [55] H. B. Zhang, Z. J. Ma, J. J. Duan, H. M. Liu, G. G. Liu, T. Wang, K. Chang, M. Li, L. Shi, X. G. Meng, K. C. Wu, J. H. Ye, *ACS Nano* **2016**, *10*, 684.
- [56] J. Ryu, N. Jung, D. H. Lim, D. Y. Shin, S. H. Park, H. C. Ham, J. H. Jang, H. J. Kim, S. J. Yoo, *Chem. Commun.* **2014**, *50*, 15940.
- [57] Y. D. Xing, X. J. Zheng, Y. H. Wu, M. R. Li, W. H. Zhang, C. Li, *Chem. Commun.* **2015**, *51*, 8146.
- [58] L. S. Chen, X. Z. Cui, Q. S. Wang, X. H. Zhang, G. Wan, F. M. Cui, C. Y. Wei, J. L. Shi, *Dalton. Trans.* **2015**, *44*, 20708.
- [59] J. W. Su, G. L. Xia, R. Li, Y. Yang, J. T. Chen, R. H. Shi, P. Jiang, Q. W. Chen, *J. Mater. Chem. A* **2016**, *4*, 9204.
- [60] J. Li, Y. C. Wang, T. Zhou, H. Zhang, X. H. Sun, J. Tang, L. J. Zhang, A. M. Al-Enizi, Z. Q. Yang, G. F. Zheng, *J. Am. Chem. Soc.* **2015**, *137*, 14305.
- [61] H. Cheng, K. Xu, L. L. Xing, S. Liu, Y. Gong, L. Gu, L. D. Zhang, C. Z. Wu, *J. Mater. Chem. A* **2016**, *4*, 11775.
- [62] E. J. Popczun, C. G. Read, C. W. Roske, N. S. Lewis, R. E. Schaak, *Angew. Chem. Int. Ed.* **2014**, *53*, 5427.
- [63] A. Mendoza-Garcia, D. Su, S. H. Sun, *Nanoscale* **2016**, *8*, 3244.
- [64] V. V. T. Doan-Nguyen, S. Zhang, E. B. Trigg, R. Agarwal, J. Li, D. Su, K. I. Winey, C. B. Murray, *ACS Nano* **2015**, *9*, 8108.
- [65] M. H. Zhuang, X. W. Ou, Y. B. Dou, L. L. Zhang, Q. C. Zhang, R. Z. Wu, Y. Ding, M. H. Shao, Z. T. Luo, *Nano Lett.* **2016**, *16*, 4691.
- [66] L. Liu, X. F. Yang, N. Ma, H. T. Liu, Y. Z. Xia, C. M. Chen, D. J. Yang, X. D. Yao, *Small* **2016**, *12*, 1295.

- [67] X. Zhong, Y. Jiang, X. L. Chen, L. Wang, G. L. Zhuang, X. N. Li, J. G. Wang, *J. Mater. Chem. A* **2016**, *4*, 10575.
- [68] A. K. Geim, I. V. Grigorieva, *Nature* **2013**, *499*, 419.
- [69] A. H. Castro Neto, K. Novoselov, *Mater. Express* **2011**, *1*, 10.
- [70] A. H. Castro Neto, K. Novoselov, *Rep. Prog. Phys.* **2011**, *74*, 8.
- [71] Y. Zheng, Y. Jiao, Y. H. Zhu, L. H. Li, Y. Han, Y. Chen, A. J. Du, M. Jaroniec, S. Z. Qiao, *Nat. Commun.* **2014**, *5*, 3783.
- [72] T. F. Jaramillo, K. P. Jorgensen, J. Bonde, J. H. Nielsen, S. Horch, I. Chorkendorff, *Science* **2007**, *317*, 100.
- [73] A. Lyalin, A. Nakayama, K. Uosaki, T. Taketsugu, *J. Phys. Chem. C* **2013**, *117*, 21359.
- [74] K. Uosaki, G. Elumalai, H. Noguchi, T. Masuda, A. Lyalin, A. Nakayama, T. Taketsugu, *J. Am. Chem. Soc.* **2014**, *136*, 6542.
- [75] W. Chen, E. J. G. Santos, W. G. Zhu, E. Kaxiras, Z. Y. Zhang, *Nano Lett.* **2013**, *13*, 509.
- [76] X. C. Wang, K. Maeda, A. Thomas, K. Takanabe, G. Xin, J. M. Carlsson, K. Domen, M. Antonietti, *Nat. Mater.* **2009**, *8*, 76.
- [77] F. Goettmann, A. Thomas, M. Antonietti, *Angew. Chem. Int. Ed.* **2007**, *46*, 2717.
- [78] T. Fu, M. Wang, W. M. Cai, Y. M. Cui, F. Gao, L. M. Peng, W. Chen, W. P. Ding, *ACS Catal.* **2014**, *4*, 2536.
- [79] X. P. Dai, Z. Z. Li, Y. D. Ma, M. Z. Liu, K. L. Du, H. X. Su, H. Y. Zhuo, L. Yu, H. Sun, X. Zhang, *ACS Appl. Mater. Interfaces* **2016**, *8*, 6439.
- [80] J. Mahmood, S. M. Jung, S. J. Kim, J. Park, J. W. Yoo, J. B. Baek, *Chem. Mater.* **2015**, *27*, 4860.
- [81] B. Liu, H. Q. Yao, R. A. Daniels, W. Q. Song, H. Q. Zheng, L. Jin, S. L. Suib, J. He, *Nanoscale* **2016**, *8*, 5441.
- [82] A. Aijaz, J. Masa, C. Rosler, W. Xia, P. Weide, A. J. R. Botz, R. A. Fischer, W. Schuhmann, M. Muhler, *Angew. Chem. Int. Ed.* **2016**, *55*, 4087.
- [83] H. T. Chung, J. H. Won, P. Zelenay, *Nat. Commun.* **2013**, *4*, 1922.
- [84] A. Q. Zhao, J. Masa, W. Xia, A. Maljusch, M. G. Willinger, G. Clavel, K. P. Xie, R. Schlogl, W. Schuhmann, M. Muhler, *J. Am. Chem. Soc.* **2014**, *136*, 7551.
- [85] W. Xia, R. Q. Zou, L. An, D. G. Xia, S. J. Guo, *Energy Environ. Sci.* **2015**, *8*, 568.
- [86] Z. Y. Wu, X. X. Xu, B. C. Hu, H. W. Liang, Y. Lin, L. F. Chen, S. H. Yu, *Angew. Chem. Int. Ed.* **2015**, *54*, 8179.
- [87] K. Strickland, M. W. Elise, Q. Y. Jia, U. Tylus, N. Ramaswamy, W. T. Liang, M. T. Sougrati, F. Jaouen, S. Mukerjee, *Nat. Commun.* **2015**, *6*, 7343.
- [88] J. S. Li, S. L. Li, Y. J. Tang, M. Han, Z. H. Dai, J. C. Bao, Y. Q. Lan, *Chem. Commun.* **2015**, *51*, 2710.
- [89] J. Wang, G. X. Wang, S. Miao, X. L. Jiang, J. Y. Li, X. H. Bao, *Carbon* **2014**, *75*, 381.
- [90] L. B. Ma, X. P. Shen, G. X. Zhu, Z. Y. Ji, H. Zhou, *Carbon* **2014**, *77*, 255.
- [91] G. Y. Zhong, H. J. Wang, H. Yu, F. Peng, *J. Power Sources* **2015**, *286*, 495.
- [92] Y. Zhang, W. J. Jiang, L. Guo, X. Zhang, J. S. Hu, Z. D. Wei, L. J. Wan, *ACS Appl. Mater. Interfaces* **2015**, *7*, 11508.
- [93] L. B. Lv, T. N. Ye, L. H. Gong, K. X. Wang, J. Su, X. H. Li, J. S. Chen, *Chem. Mater.* **2015**, *27*, 544.
- [94] J. B. Xi, Y. T. Xia, Y. Y. Xu, J. W. Xiao, S. Wang, *Chem. Commun.* **2015**, *51*, 10479.
- [95] Y. L. Liu, X. Y. Xu, P. C. Sun, T. H. Chen, *Int. J. Hydrogen Energy* **2015**, *40*, 4531.
- [96] H. L. Tang, S. C. Cai, S. L. Xie, Z. B. Wang, Y. X. Tong, M. Pan, X. H. Lu, *Adv. Sci.* **2016**, *3*, 1500265.
- [97] H. L. Jiang, Y. F. Yao, Y. H. Zhu, Y. Y. Liu, Y. H. Su, X. L. Yang, C. Z. Li, *ACS Appl. Mater. Interfaces* **2015**, *7*, 21511.
- [98] X. Zhong, L. Liu, Y. Jiang, X. D. Wang, L. Wang, G. L. Zhuang, X. N. Li, D. H. Mei, J. G. Wang, D. S. Su, *ChemCatChem* **2015**, *7*, 1826.
- [99] D. W. Ma, S. W. Jia, D. Q. Zhao, Z. S. Lu, Z. X. Yang, *Appl. Surf. Sci.* **2014**, *300*, 91.
- [100] J. Y. Li, J. Wang, D. F. Gao, X. Y. Li, S. Miao, G. X. Wang, X. H. Bao, *Catal. Sci. Technol.* **2016**, *6*, 2949.
- [101] C. Y. Mao, A. G. Kong, Y. Wang, X. H. Bu, P. Y. Feng, *Nanoscale* **2015**, *7*, 10817.
- [102] Y. Z. Wu, J. B. Zang, L. Dong, Y. Zhang, Y. H. Wang, *J. Power Sources* **2016**, *305*, 64.
- [103] Z. X. Wu, J. Wang, L. L. Han, R. Q. Lin, H. F. Liu, H. L. L. Xin, D. L. Wang, *Nanoscale* **2016**, *8*, 4681.
- [104] S. L. Zhang, Y. Zhang, W. J. Jiang, X. Liu, S. L. Xu, R. J. Huo, F. Z. Zhang, J. S. Hu, *Carbon* **2016**, *107*, 162.
- [105] Y. Hu, L. J. Zhong, J. O. Jensen, Q. F. Li, *Asia-Pac. J. Chem. Eng.* **2016**, *11*, 382.
- [106] Z. J. Wang, B. Li, X. M. Ge, F. W. T. Goh, X. Zhang, G. J. Du, D. Wu, Z. L. Liu, T. S. A. Hor, H. Zhang, Y. Zong, *Small* **2016**, *12*, 2580.
- [107] G. Zhang, W. T. Lu, F. F. Cao, Z. D. Xiao, X. S. Zheng, *J. Power Sources* **2016**, *302*, 114.
- [108] T. Cao, D. S. Wang, J. T. Zhang, C. B. Cao, Y. D. Li, *Chem.-Eur. J.* **2015**, *21*, 14022.
- [109] H. Feng, L. Wang, L. Zhao, C. G. Tian, P. Yu, H. G. Fu, *Phys. Chem. Chem. Phys.* **2016**, *18*, 26572.
- [110] Y. Hu, J. O. Jensen, W. Zhang, L. N. Cleemann, W. Xing, N. J. Bjerrum, Q. F. Li, *Angew. Chem. Int. Ed.* **2014**, *53*, 3675.
- [111] Y. Y. Liu, H. L. Jiang, Y. H. Zhu, X. L. Yang, C. Z. Li, *J. Mater. Chem. A* **2016**, *4*, 1694.
- [112] A. G. Kong, C. Y. Mao, Q. P. Lin, X. Wei, X. H. Bu, P. Y. Feng, *Dalton Trans.* **2015**, *44*, 6748.
- [113] Y. Hu, J. O. Jensen, W. Zhang, S. Martin, R. Chenitz, C. Pan, W. Xing, N. J. Bjerrum, Q. F. Li, *J. Mater. Chem. A* **2015**, *3*, 1752.
- [114] W. J. Jiang, L. Gu, L. Li, Y. Zhang, X. Zhang, L. J. Zhang, J. Q. Wang, J. S. Hu, Z. D. Wei, L. J. Wan, *J. Am. Chem. Soc.* **2016**, *138*, 3570.
- [115] W. X. Yang, X. J. Liu, X. Y. Yue, J. B. Jia, S. J. Guo, *J. Am. Chem. Soc.* **2015**, *137*, 1436.
- [116] W. X. Yang, X. Y. Yue, X. J. Liu, L. L. Chen, J. B. Jia, S. J. Guo, *Nanoscale* **2016**, *8*, 959.
- [117] Y. Zhang, L. B. Huang, W. J. Jiang, X. Zhang, Y. Y. Chen, Z. D. Wei, L. J. Wan, J. S. Hu, *J. Mater. Chem. A* **2016**, *4*, 7781.
- [118] Y. Hou, S. M. Cui, Z. H. Wen, X. R. Guo, X. L. Feng, J. H. Chen, *Small* **2015**, *11*, 5940.
- [119] S. H. Noh, M. H. Seo, X. Ye, Y. Makinose, T. Okajima, N. Matsushita, B. Han, T. Ohsaka, *J. Mater. Chem. A* **2015**, *3*, 22031.
- [120] M. Tavakkoli, T. Kallio, O. Reynaud, A. G. Nasibulin, C. Johans, J. Sainio, H. Jiang, E. I. Kauppinen, K. Laasonen, *Angew. Chem. Int. Ed.* **2015**, *54*, 4535.
- [121] Y. Wang, Y. Nie, W. Ding, S. G. Chen, K. Xiong, X. Q. Qi, Y. Zhang, J. Wang, Z. D. Wei, *Chem. Commun.* **2015**, *51*, 8942.
- [122] H. L. Fei, Y. Yang, Z. W. Peng, G. D. Ruan, Q. F. Zhong, L. Li, E. L. G. Samuel, J. M. Tour, *ACS Appl. Mater. Interfaces* **2015**, *7*, 8083.
- [123] J. Wang, G. X. Wang, S. Miao, J. Y. Li, X. H. Bao, *Faraday Discuss.* **2014**, *176*, 135.
- [124] S. P. Wang, J. Wang, M. L. Zhu, X. B. Bao, B. Y. Xiao, D. F. Su, H. R. Li, Y. Wang, *J. Am. Chem. Soc.* **2015**, *137*, 15753.
- [125] S. Zhang, X. B. Yu, F. Yan, C. Y. Li, X. T. Zhang, Y. J. Chen, *J. Mater. Chem. A* **2016**, *4*, 12046.
- [126] B. R. Liu, L. Zhang, W. L. Xiong, M. M. Ma, *Angew. Chem. Int. Ed.* **2016**, *55*, 6724.
- [127] L. Han, M. Xu, Y. J. Han, Y. Yu, S. J. Dong, *ChemSusChem* **2016**, *9*, 2784.
- [128] H. Y. Jin, J. Wang, D. F. Su, Z. Z. Wei, Z. F. Pang, Y. Wang, *J. Am. Chem. Soc.* **2015**, *137*, 2688.
- [129] Y. Hou, Z. H. Wen, S. M. Cui, S. Q. Ci, S. Mao, J. H. Chen, *Adv. Funct. Mater.* **2015**, *25*, 872.

- [130] S. Gao, G. D. Li, Y. P. Liu, H. Chen, L. L. Feng, Y. Wang, M. Yang, D. J. Wang, S. Wang, X. X. Zou, *Nanoscale* **2015**, 7, 2306.
- [131] X. J. Fan, Z. W. Peng, R. Q. Ye, H. Q. Zhou, X. Guo, *ACS Nano* **2015**, 9, 7407.
- [132] Y. Yang, Z. Y. Lun, G. L. Xia, F. C. Zheng, M. N. He, Q. W. Chen, *Energy Environ. Sci.* **2015**, 8, 3563.
- [133] T. Wang, Q. Y. Zhou, X. J. Wang, J. Zheng, X. G. Li, *J. Mater. Chem. A* **2015**, 3, 16435.
- [134] S. Gao, Y. P. Liu, G. D. Li, Y. C. Guo, Y. C. Zou, X. X. Zou, *Electrochim. Acta* **2016**, 199, 99.
- [135] F. C. Zheng, H. Y. Xia, S. H. Xu, R. C. Wang, Y. G. Zhang, *RSC Adv.* **2016**, 6, 71767.
- [136] Z. H. Pu, X. Ya, I. S. Amiin, Z. K. Tu, X. B. Liu, W. Q. Li, S. C. Mu, *J. Mater. Chem. A* **2016**, 4, 15327.
- [137] Y. Zhou, R. G. Ma, P. X. Li, Y. F. Chen, Q. Liu, G. Z. Cao, J. C. Wang, *J. Mater. Chem. A* **2016**, 4, 8204.
- [138] J. S. Li, Y. Wang, C. H. Liu, S. L. Li, Y. G. Wang, L. Z. Dong, Z. H. Dai, Y. F. Li, Y. Q. Lan, *Nat. Commun.* **2016**, 7, 11204.
- [139] X. X. Zou, X. X. Huang, A. Goswami, R. Silva, B. R. Sathe, E. Mikmekova, T. Asefa, *Angew. Chem., Int. Ed.* **2014**, 53, 4372.
- [140] W. J. Zhou, J. Zhou, Y. C. Zhou, J. Lu, K. Zhou, L. J. Yang, Z. H. Tang, L. G. Li, S. W. Chen, *Chem. Mater.* **2015**, 27, 2026.
- [141] H. Su, H. H. Wang, B. Zhang, K. X. Wang, X. H. Li, J. S. Chen, *Nano Energy* **2016**, 22, 79.
- [142] W. J. Zhou, T. L. Xiong, C. H. Shi, J. Zhou, K. Zhou, N. W. Zhu, L. G. Li, Z. H. Tang, S. W. Chen, *Angew. Chem. Int. Ed.* **2016**, 55, 8416.
- [143] M. S. Faber, S. Jin, *Energy Environ. Sci.* **2014**, 7, 3519.
- [144] C. G. Morales-Guio, L. A. Stern, X. L. Hu, *Chem. Soc. Rev.* **2014**, 43, 6555.
- [145] Y. P. Liu, G. T. Yu, G. D. Li, Y. H. Sun, T. Asefa, W. Chen, X. X. Zou, *Angew. Chem. Int. Ed.* **2015**, 54, 10752.
- [146] R. G. Ma, Y. Zhou, Y. F. Chen, P. X. Li, Q. Liu, J. C. Wang, *Angew. Chem., Int. Ed.* **2015**, 54, 14723.
- [147] W. C. Ellis, N. D. McDaniel, S. Bernhard, T. J. Collins, *J. Am. Chem. Soc.* **2010**, 132, 10990.
- [148] Q. S. Yin, J. M. Tan, C. Besson, Y. V. Geletii, D. G. Musaev, A. E. Kuznetsov, Z. Luo, K. I. Hardcastle, C. L. Hill, *Science* **2010**, 328, 342.
- [149] Z. Y. Lu, H. T. Wang, D. S. Kong, K. Yan, P. C. Hsu, G. Y. Zheng, H. B. Yao, Z. Liang, X. M. Sun, Y. Cui, *Nat. Commun.* **2014**, 5, 4345.
- [150] B. Y. Xia, Y. Yan, N. Li, H. B. Wu, X. W. Lou, X. Wang, *Nat. Energy* **2016**, 1, 15006.
- [151] X. Zhang, H. M. Xu, X. X. Li, Y. Y. Li, T. B. Yang, Y. Y. Liang, *ACS Catal.* **2016**, 6, 580.
- [152] Y. F. Zhao, J. Q. Zhang, K. F. Li, Z. M. Ao, C. Y. Wang, H. Liu, K. N. Sun, G. X. Wang, *J. Mater. Chem. A* **2016**, 4, 12818.
- [153] D. H. Won, H. Shin, J. Koh, J. Chung, H. S. Lee, H. Kim, S. I. Woo, *Angew. Chem. Int. Ed.* **2016**, 55, 9297.
- [154] S. Gao, Y. Lin, X. C. Jiao, Y. F. Sun, Q. Q. Luo, W. H. Zhang, D. Q. Li, J. L. Yang, Y. Xie, *Nature* **2016**, 529, 68.
- [155] Z. L. Wang, C. L. Li, Y. Yamauchi, *Nano Today* **2016**, 11, 373.
- [156] H. B. Zhang, T. Wang, J. J. Wang, H. M. Liu, T. D. Dao, M. Li, G. G. Liu, X. G. Meng, K. Chang, L. Shi, T. Nagao, J. H. Ye, *Adv. Mater.* **2016**, 28, 3703.
- [157] J. Balamurugan, T. D. Thanh, N. H. Kim, J. H. Lee, *Adv. Mater. Interfaces* **2016**, 3, 1500348.
- [158] M. S. Wu, Z. Z. Ceng, *Electrochim. Acta* **2016**, 191, 895.
- [159] P. P. Sun, M. Zhang, C. Z. Ai, Z. X. Wu, S. Lu, X. T. Zhang, N. Huang, Y. H. Sun, X. H. Sun, *J. Power Sources* **2016**, 319, 219.
- [160] X. J. Zheng, J. Deng, N. Wang, D. H. Deng, W. H. Zhang, X. H. Bao, C. Li, *Angew. Chem. Int. Ed.* **2014**, 53, 7023.
- [161] C. Y. Zhu, F. Xu, J. Chen, H. H. Min, H. Dong, L. Tong, K. Qasim, S. L. Li, L. T. Sun, *J. Power Sources* **2016**, 303, 159.
- [162] M. S. Wu, Z. Z. Ceng, C. Y. Chen, C. Wang, *J. Alloy Compd.* **2016**, 688, 342.
- [163] K. Saranya, A. Subramania, N. Sivasankar, *RSC Adv.* **2015**, 5, 43611.
- [164] M. S. Wu, C. Y. Chen, Y. R. Chen, H. C. Shih, *Electrochim. Acta* **2016**, 215, 50.
- [165] Y. G. Li, H. J. Dai, *Chem. Soc. Rev.* **2014**, 43, 5257.
- [166] Z. L. Wang, D. Xu, J. J. Xu, X. B. Zhang, *Chem. Soc. Rev.* **2014**, 43, 7746.
- [167] Y. J. Ding, Y. C. Niu, J. Yang, L. Ma, J. G. Liu, Y. J. Xiong, H. X. Xu, *Small* **2016**, 12, 5414.
- [168] M. Zeng, Y. L. Liu, F. P. Zhao, K. Q. Nie, N. Han, X. X. Wang, W. J. Huang, X. N. Song, J. Zhong, Y. G. Li, *Adv. Funct. Mater.* **2016**, 26, 4397.
- [169] J. B. Zhu, M. L. Xiao, Y. L. Zhang, Z. Jin, Z. Q. Peng, C. P. Liu, S. L. Chen, J. J. Ge, W. Xing, *ACS Catal.* **2016**, 6, 6335.
- [170] J. Wang, H. H. Wu, D. F. Gao, S. Miao, G. X. Wang, X. H. Bao, *Nano Energy* **2015**, 13, 387.
- [171] P. G. Bruce, S. A. Freunberger, L. J. Hardwick, J. M. Tarascon, *Nat. Mater.* **2012**, 11, 19.
- [172] Z. Q. Peng, S. A. Freunberger, Y. H. Chen, P. G. Bruce, *Science* **2012**, 337, 563.
- [173] S. H. Oh, R. Black, E. Pomerantseva, J. H. Lee, L. F. Nazar, *Nat. Chem.* **2012**, 4, 1004.
- [174] J. S. Hummelshøj, A. C. Luntz, J. K. Nørskov, *J. Chem. Phys.* **2013**, 138, 034703.
- [175] R. Black, J. H. Lee, B. Adams, C. A. Mims, L. F. Nazar, *Angew. Chem. Int. Ed.* **2013**, 52, 392.
- [176] L. Grande, E. Paillard, J. Hassoun, J. B. Park, Y. J. Lee, Y. K. Sun, S. Passerini, B. Scrosati, *Adv. Mater.* **2015**, 27, 784.
- [177] Y. C. Tu, H. B. Li, D. H. Deng, J. P. Xiao, X. J. Cui, D. Ding, M. S. Chen, X. H. Bao, *Nano Energy* **2016**, 30, 877.
- [178] X. W. Guo, P. Liu, J. H. Han, Y. Ito, A. Hirata, T. Fujita, M. W. Chen, *Adv. Mater.* **2015**, 27, 6137.
- [179] X. Huang, H. Yu, H. T. Tan, J. X. Zhu, W. Y. Zhang, C. Y. Wang, J. Zhang, Y. X. Wang, Y. B. Lv, Z. Zeng, D. Y. Liu, J. Ding, Q. C. Zhang, M. Srinivasan, P. M. Ajayan, H. H. Hng, Q. Y. Yan, *Adv. Funct. Mater.* **2014**, 24, 6516.
- [180] L. Hu, R. R. Zhang, L. Z. Wei, F. P. Zhang, Q. W. Chen, *Nanoscale* **2015**, 7, 450.
- [181] X. Y. Li, C. M. Zeng, J. Jiang, L. H. Ai, *J. Mater. Chem. A* **2016**, 4, 7476.
- [182] J. L. Long, K. Shen, L. Chen, Y. W. Li, *J. Mater. Chem. A* **2016**, 4, 10254.
- [183] A. L. M. da Silva, J. P. den Breejen, L. V. Mattos, J. H. Bitter, K. P. de Jong, F. B. Noronha, *J. Catal.* **2014**, 318, 67.
- [184] J. Lee, O. K. Farha, J. Roberts, K. A. Scheidt, S. T. Nguyen, J. T. Hupp, *Chem. Soc. Rev.* **2009**, 38, 1450.
- [185] V. K. Mittal, S. Bera, T. Saravanan, S. Sumathi, R. Krishnan, S. Rangarajan, S. Velmurugan, S. V. Narasimhan, *Thin Solid Films* **2009**, 517, 1672.
- [186] B. V. A. Rao, M. Y. Iqbal, B. Sreedhar, *Corros. Sci.* **2009**, 51, 1441.
- [187] B. Wang, M. Caffio, C. Bromley, H. Fruchtl, R. Schaub, *ACS Nano* **2010**, 4, 5773.
- [188] X. Q. Chen, D. H. Deng, X. L. Pan, X. H. Bao, *Chin. J. Catal.* **2015**, 36, 1631.
- [189] C. Wang, P. Zhai, Z. C. Zhang, Y. Zhou, J. Ju, Z. J. Shi, D. Ma, R. P. S. Han, F. Q. Huang, *Part. Part. Syst. Character.* **2015**, 32, 29.
- [190] C. Wang, P. Zhai, Z. C. Zhang, Y. Zhou, J. K. Zhang, H. Zhang, Z. J. Shi, R. P. S. Han, F. Q. Huang, D. Ma, *J. Catal.* **2016**, 334, 42.